

A new model for dilute polymer solutions in flows with strong extensional components

Indranil Ghosh, Yong Lak Joo,^{a)} Gareth H. McKinley,^{b)} Robert A. Brown,
and Robert C. Armstrong^{c)}

*Department of Chemical Engineering, Massachusetts Institute of Technology,
Cambridge, Massachusetts 02139-4307*

(Received 31 August 2001; final revision received 26 June 2002)

Synopsis

Ghosh *et al.* (2001) demonstrated that the Kramers chain captures the optical and rheological properties of dilute polymer solutions in rapidly varying elongational flows better than the finitely extensible nonlinear elastic dumbbell model. A new model, based on introducing an adaptive length scale (ALS) as an internal variable, is developed to reproduce the fine scale physics of the Kramers chain. The resulting ALS-model describes the polymer molecule as a set of identical segments in which each segment represents a fragment of the polymer that is short enough so that it can sample its entire configuration space on the time scale of an imposed deformation and, therefore, stretch reversibly. As the molecule unravels, the number of segments decreases, but the maximum length of each segment increases, so that the constant maximum contour length of the molecule is preserved. The ALS model gives very good predictions of stress growth in startup of uniaxial elongation and stress-birefringence hysteresis in a uniaxial elongational flow followed by relaxation. A closed form of the constitutive equation, the ALS-C model, is proposed. The rheological predictions of the ALS-C model resemble those of the ALS equation. This coupled with its small number of internal degrees of freedom suggests that this constitutive equation may be useful in modeling complex flows. © 2002 The Society of Rheology. [DOI: 10.1122/1.1501963]

I. INTRODUCTION

Several researchers [for example Coates *et al.* (1992), Purnode *et al.* (1996), Liu *et al.* (1998), and Talwar and Khomami (1995)] have demonstrated disagreement between flow simulations and experimental measurements in complex geometries. They have suggested that the discrepancies may be due to inadequacies of the constitutive equations that are used in the flow simulations. The most commonly used constitutive equations are derived from elastic dumbbell models, such as the Hookean dumbbell and finitely extensible nonlinear elastic (FENE) dumbbell models. Constitutive equations based on dumbbell models are inexpensive to use in numerical simulations, because these models have only one configurational variable, namely, the end-to-end vector of the dumbbell. However, evidence suggests that these one-mode models poorly predict the experimentally observed behavior of polymer solutions in the startup of extensional flow [James *et al.* (1995); Tirtaatmadja *et al.* (1995); Herrchen *et al.* (1997); Doyle *et al.* (1998a); and

^{a)}Current address: School of Chemical and Biomolecular Engineering, Cornell University, Ithaca, NY 14853.

^{b)}Department of Mechanical Engineering.

^{c)}Author to whom correspondence should be addressed; electronic mail: rca@mit.edu

Ghosh *et al.* (2001)]. These results demonstrate the great need for a molecular model with a small number of configurational variables that accurately mimics the multimode behavior of a polymer chain in numerical simulations of complex flows. In this paper we develop such a model.

The new model is built by first understanding the dynamics of a fine grain model, the Kramers chain, and then incorporating the physical insights from this model into the simpler framework of a bead-spring model. Through this systematic approach to coarse graining, we develop a model that is consistent with the fine scale physics of a polymer chain subjected to a wide range of flows. Several important aspects of Kramers chain dynamics in a uniaxial extensional flow have already been presented in Ghosh *et al.* (2001). Through simulations of the Kramers chain, we demonstrated that the effective end-to-end force in a polymer chain deviates from the previously proposed *dumbbell* force laws in strong extensional flows. In particular, for a given value of the end-to-end distance, the effective force varies with strain and strain rate. This is dramatically different from a dumbbell with an inverse Langevin force law [Flory (1953)]. The inverse Langevin force law (or the Warner approximation to it) describes the entropic elasticity in a slowly stretching polymer chain and is independent of the strain or strain rate imparted by the flow. Even the force law in the Verhoef dumbbell [Verhoef *et al.* (1999)], which depends on strain rate, does not describe the complex behavior of the effective end-to-end force of the Kramers chain because it does not contain the correct strain dependence. In Ghosh *et al.* (2001), it was concluded that the complexity of the effective force would be very difficult to capture in a simple, analytical form. It was suggested that alternative strategies be attempted to improve upon existing dumbbell models.

In this paper, we do not try to derive a new force law for a bead-spring dumbbell. Instead, we observe that there is a maximum number of segments that may be modeled accurately as an entropic spring in any given deformation and that this number depends upon the strain rate and strain. We use this information to develop a one-mode bead-spring model with a length scale that evolves adaptively with the kinematical history. For small strains, the adaptive length scale is small and allows the model to capture short length scale effects that are missed by the FENE dumbbell. Conversely, at large strains, the adaptive length scale approaches the maximum contour length in order to represent chains that are almost fully unraveled. The new model, referred to as the adaptive length scale (ALS) model, is formulated as a set of stochastic differential equations, which are solved by using standard Brownian dynamics methods [Öttinger (1996)].

This paper is organized as follows. Section II summarizes existing models, such as the Kramers chain and FENE chain; the behavior of the ALS model is compared extensively with these models. The new model is developed in Secs. III to V, and is tested in a wide variety of kinematics in Secs. VI and VII. Finally, a closed form constitutive equation based on the Peterlin approximation, the ALS-C model is reported in Sec. VIII. This form may be particularly useful in numerical simulations of complex flows.

II. EXISTING MODELS AND SIMULATION TECHNIQUES

The principal ideas behind some common polymer models are briefly reviewed in this section. A more detailed discussion is found in Ghosh *et al.* (2001). Here we present the most important relations and introduce the notation that is used in the remainder of the paper.

A flexible, linear polymer molecule of molecular weight M_w and characteristic ratio factor C_∞ can be represented by a bead-rod or Kramers chain that consists of N beads

connected by $(N-1)$ rods each of length a . Flory [(1953); cf. pp. 411–414, Chap. X] shows that the number of rods is given by

$$N-1 = \frac{2M_w \sin^2(\theta/2)}{M_0 C_\infty} \quad (1)$$

where M_0 is the monomer molecular weight and the length of each rod is given by

$$a = \frac{C_\infty l}{\sin(\theta/2)}, \quad (2)$$

where l is the length of a carbon–carbon bond and θ is the angle between carbon–carbon bonds in the polymer backbone. The time constant λ_d of the polymer molecule is found by measuring the ratio of the zero-shear-rate first normal stress coefficient to the zero-shear-rate polymer contribution to viscosity as

$$\frac{\Psi_{1,0}}{2(\eta_0 - \eta_s)} = \lambda_d. \quad (3)$$

The time constant is related to the number of rods in a Kramers chain representation by [Doyle (1997)]

$$\lambda_d = 0.0142 N^2 \frac{\zeta a^2}{kT}, \quad (4)$$

where ζ represents the drag coefficient of a bead. Since it is difficult to estimate the drag coefficient on a bead *a priori*, it can be calculated from Eq. (4), if required.

The equation of motion for the ν th bead in the chain is given by

$$\dot{\mathbf{r}}_\nu = \mathbf{v}_0 + [\boldsymbol{\kappa} \cdot \mathbf{r}_\nu] + \frac{1}{\zeta} \mathbf{F}_\nu^{(c)} + \frac{1}{\zeta} \mathbf{F}_\nu^{(b)}, \quad (5)$$

where \mathbf{v}_0 is the velocity of the solvent field at a fixed, arbitrary origin, $\dot{\mathbf{r}}_\nu$ is the velocity of the ν th bead, $\boldsymbol{\kappa}$ is the transpose of the velocity gradient tensor, and \mathbf{r}_ν is the bead position vector. The first two terms on the right-hand side derive from the hydrodynamic drag felt by the ν th bead, and $\mathbf{F}_\nu^{(b)}$ and $\mathbf{F}_\nu^{(c)}$ represent the Brownian and constraint forces, respectively. The constraint forces are calculated to keep the rods of fixed length a .

The stress is calculated from the Giesekus equation (Bird *et al.*, 1987) as

$$\tau_p = \frac{1}{2} n_p \zeta \sum_{\nu=1}^N \langle \mathbf{R}_\nu \mathbf{R}_\nu \rangle_{(1)}, \quad (6)$$

where \mathbf{R}_ν is the position of bead ν with respect to the center of mass of the molecule, the subscript (1) denotes the (upper) convected derivative, and n_p is the number density of the polymers in solution. The expression for the birefringence [Doyle (1997)] is

$$\Delta n = 5Cn_p kT \sum_{\nu=1}^{N-1} \langle u_{\nu z} u_{\nu z} - u_{\nu x} u_{\nu x} \rangle, \quad (7)$$

where

$$C = \frac{2\pi}{45kT} \frac{(n^2+2)^2}{n} (\alpha_1 - \alpha_2) \quad (8)$$

and n is the isotropic part of the refractive index tensor, (α_1, α_2) are the (parallel, perpendicular) components of the polarizability tensor, and $(u_{\nu x}, u_{\nu z})$ are the (x, z) components of the unit vector pointing from the ν th to the $(\nu+1)$ th bead.

An important dimensionless quantity in a uniaxial elongational flow is the Weissenberg number, which is the product of the time constant of the molecule and the elongation rate

$$\text{Wi} = 0.0142N^2 \frac{\zeta a^2}{kT} \dot{\varepsilon}. \quad (9)$$

Brownian dynamics simulations of the Kramers chains were conducted by using the algorithm of Liu (1989).

Bead-spring models are coarse-grained approximations to the Kramers chain in which the entropic elasticity of subsections of the chain is represented by springs. The spring force is directed along the vector \mathbf{Q} connecting two adjacent beads, and the magnitude of the force is a function of the bead separation. For small extensions of the spring, the force is linear in the bead separation, the proportionality constant H being related to the parameters of the Kramers chain by

$$H = \frac{3MkT}{(N-1)a^2}, \quad (10)$$

where M is the number of equal length springs used to represent the Kramers chain. For large extensions, the force law becomes nonlinear. Flory (1953) has shown that the force required to hold the ends of the chain at a fixed separation is given by the inverse Langevin function. It has been experimentally verified by direct measurements on flexible polystyrene molecules that the inverse Langevin function is a good approximation to the entropic elastic force in a flexible chain [Ortiz *et al.* (1999)]. An approximation to this function, which is more computationally tractable, was developed by Warner and is referred to as the FENE (finitely extensible nonlinear elastic) force law. The FENE force law is given by the simple analytical form

$$F^{(\text{FENE})}(Q) = \frac{HQ}{1 - (Q/Q_0)^2}, \quad (11)$$

where Q_0 is the maximum extension of each spring and is given by

$$Q_0 = \frac{(N-1)}{M} a. \quad (12)$$

The maximum extensibility of each spring is often expressed by the parameter b , which is defined as

$$b = \frac{HQ_0^2}{kT} \quad (13)$$

and gives the square of the ratio of the maximum to equilibrium length of the spring. Substituting Eqs. (10) and (12) into Eq. (13) yields the relationship

$$b = \frac{3(N-1)}{M}. \quad (14)$$

Thus, a Kramers chain of $(N-1)$ rods can be compared with a FENE chain with M springs, each with a value of b given by Eq. (14).

The inverse Langevin force law (and the FENE approximation) assumes that for a given end-to-end distance, a Kramers chain has sufficient time to sample its entire conformational space and that the internal conformational distribution has reached equilibrium. This force law should, therefore, be used with caution in nonequilibrium situations. Only when the time scale of the deformation is much longer than the relaxation time scale of the entire chain does the chain unravel reversibly (i.e., the internal conformation distribution of the chain is able to equilibrate at each stage of the stretching).

The spring force $\mathbf{F}^{(s)}$ is required to calculate the stress for bead-spring models with the Kramers expression for the stress tensor

$$\tau_p = M n_p kT \delta - n_p \sum_{i=1}^M \langle \mathbf{Q}_i \mathbf{F}_i^{(s)} \rangle, \quad (15)$$

where for FENE chains $\mathbf{F}^{(s)}$ is set to $\mathbf{F}^{(\text{FENE})}$. The birefringence of bead-spring models is calculated from the expression of Wiest (1999) as

$$\Delta n = n_p (\alpha_1 - \alpha_2) \frac{2\pi}{9} \frac{(n^2+2)^2}{n} \frac{n_s}{Q_0^2} \sum_{i=1}^M \langle Q_{iz} Q_{iz} - Q_{ix} Q_{ix} \rangle, \quad (16)$$

where each spring corresponds to n_s rods in the Kramers chain representation of the polymer. The time constant λ , for an individual spring is $\zeta_s/4H$, where ζ_s is the hydrodynamic drag on a bead in the FENE chain. This time constant can be related to the time constant of the entire molecule through the scaling relationship suggested in Ghosh *et al.* (2001):

$$\lambda_s = \frac{\zeta_s}{4H} = \frac{\lambda_d}{K}, \quad (17)$$

where

$$K = \left(\frac{b}{b+5} \right) \left(\frac{\sqrt{(b_{\max}+5)(b_{\max}+7)}}{b_{\max}} \right) \left\{ \frac{[2(M+1)^2+7][(M+1)^2-1]}{45} - \frac{12[(M+1)^2+1][(M+1)^2-1]}{45(M+1)(b+7)} \right\}^{1/2} \quad (18)$$

and b_{\max} is the finite extensibility of a FENE dumbbell representing the entire molecule. The Brownian dynamics algorithm used to simulate the FENE chains is identical to that of van den Brule (1993).

III. REPRESENTATION OF POLYMER MOLECULES BY THE NEW MODEL

Figure 1 compares the stress growth in uniaxial extension at $Wi = 11.4$ for a 40-link Kramers chain and a FENE spring chain that represent a polymer molecule of the same maximum extension. The time constant of the overall molecule λ_d is assumed to be the same for each of the FENE chains, independent of the number of segments used to represent the polymer. Accordingly, the time constant of each spring in the FENE chain is scaled according to Eq. (17). Since the spring constant is inversely proportional to the number of Kramers rods the spring represents, as indicated in Eq. (10), Eq. (17) also describes the scaling of the drag coefficient of a bead in the FENE chain with M . Figure

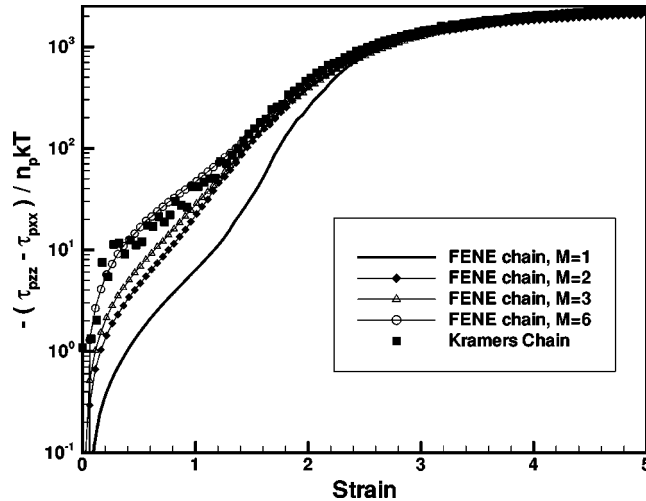


FIG. 1. Uniaxial extension at $\text{Wi} = 11.4$ for a 40-rod Kramers chain and equivalent FENE chains.

1 is reproduced from Ghosh *et al.* (2001) where it was used to support the scaling of the drag presented in Sec. II. In this paper it is used to guide us in developing an efficient way to model the dynamics of a polymer chain.

Though a Kramers chain is arguably the best mesoscale molecular model for describing the physics of a dilute polymer solution, its many internal degrees of freedom makes it a computationally expensive model in complex flow simulations. In contrast, a FENE dumbbell is much more tractable computationally, but as shown in Fig. 1, it predicts the short time scale behavior poorly. Since a FENE chain with six springs can capture the short length scale behavior with much less computational effort than the Kramers chain, the FENE chain may seem to be the most efficient way to model a polymer molecule. However, there are two reasons why this is not the case. First, multiple springs are required to describe the polymer for the first unit of strain, but for $\epsilon > 3$, the FENE dumbbell performs adequately. Therefore, the use of FENE chains at large strains is inefficient because a single spring would suffice. Second, we know of no systematic way to map between FENE chains with different numbers of springs. For example, if we want to switch from a 6-mode model to a 1-mode model at $\epsilon = 3$, we lack the methodology to do so. In a complex flow, the problem is more severe, because the strength of deformation varies spatially. In slowly deforming regions, only a few modes are needed, but a large number of modes might be needed throughout the geometry in order to resolve the behavior in parts of the domain where the polymer experiences rapid deformations. A more efficient way to model polymer dynamics, therefore, would be to develop a model with a single spring whose length scale adapts according to the kinematical history. In this paper, we develop a new adaptive length scale model motivated by a mechanistic understanding of the behavior of a Kramers chain rather than develop a systematic theory to map between fine and coarse-grained models.

We define the adaptive length scale as the contour length of a fragment of the polymer chain over which the inverse Langevin function describes the end-to-end force of the fragment. Let us consider the evolution of the adaptive length scale in the startup of a rapid uniaxial elongation. We first describe the behavior of the adaptive length scale at low strains. If $\psi(\mathbf{x}|Q, t)$ represents the configurational distribution function of Kramers chains with end-to-end distance Q at time t , then the end-to-end force of these Kramers

chains is given by the inverse Langevin function if $\psi(\mathbf{x}|Q,t) = \psi_{\text{eq}}(\mathbf{x}|Q)$. Here, $\mathbf{x} = \{\mathbf{r}_1, \mathbf{r}_2, \dots, \mathbf{r}_N\}$ is the full set of configurational variables specifying the locations of all of the beads. By definition, $\psi(\mathbf{x}|Q,t)$ is equal to $\psi_{\text{eq}}(\mathbf{x}|Q)$ in a quiescent fluid. Consequently, the inverse Langevin function describes the end-to-end force for the overall molecule, and the adaptive length scale equals the contour length of the entire molecule. If a rapid elongational flow (large $\dot{\epsilon}$) is suddenly applied for a small strain ϵ_1 then the distribution function $\psi(\mathbf{x}|Q,t)$ is different from that corresponding to equilibrium, because the internal configurations of the molecules are distorted so rapidly by the flow that they are unable to re-equilibrate on the time scale $\dot{\epsilon}^{-1}$ of the deformation. As demonstrated by Ghosh *et al.* (2001), the discrepancy between $\psi(\mathbf{x}|Q,t)$ and $\psi_{\text{eq}}(\mathbf{x}|Q)$, results in the inability of the inverse Langevin function to describe the end-to-end force of the molecules in this flow situation. As the fluid is elongated to a larger strain, $\epsilon_2 > \epsilon_1$, the deviation of $\psi(\mathbf{x}|Q,t)$ from equilibrium increases, as does the deviation of the end-to-end force from the inverse Langevin function.

Let us now consider a fragment of the above Kramers chains, say from the first to the p th bead. We denote the configurational distribution function for molecules which have end-to-end distance Q and for which the distance between the first and p th beads is Q_f as $\psi_f(\mathbf{x}_f|Q_f,Q,t)$, where $\mathbf{x}_f = \{\mathbf{r}_1, \mathbf{r}_2, \dots, \mathbf{r}_p\}$. At equilibrium, this contracted distribution function assumes its equilibrium value $\psi_{f,\text{eq}}(\mathbf{x}_f|Q_f,Q,t)$, but when the fluid is elongated to strain ϵ_1 at large $\dot{\epsilon}$, $\psi_f(\mathbf{x}_f|Q_f,Q,t)$ deviates from equilibrium. However, since this fragment of the molecule has a smaller time constant than the overall molecule, it is able to re-equilibrate to a greater extent than the entire molecule on the time scale of the deformation $\dot{\epsilon}^{-1}$. Consequently, the difference between $\psi_f(\mathbf{x}_f|Q_f,Q,t)$ and $\psi_{f,\text{eq}}(\mathbf{x}_f|Q_f,Q,t)$ is smaller than that between $\psi(\mathbf{x}|Q,t)$ and its corresponding equilibrium distribution function at strain ϵ_1 . Therefore, the inverse Langevin function better approximates the end-to-end force of this segment than the end-to-end force of the entire molecule.

Following this argument, *there exists a fragment of the molecule that is sufficiently small such that it is locally equilibrated when undergoing rapid elongation at strain rate $\dot{\epsilon}$ up to strain ϵ_1* . We postulate that a fragment of the polymer that satisfies the condition $\lambda_f \dot{\epsilon} = 1$, where λ_f is the time constant of the fragment, is *locally equilibrated*. The contour length of the fragment is defined as the adaptive length scale at strain ϵ_1 , because the inverse Langevin function can describe the end-to-end force over this length scale. Since the configurational distribution function of the molecule $\psi(\mathbf{x}|Q,t)$ does not change discontinuously upon the sudden inception of rapid elongational flow, the adaptive length scale similarly decreases continuously from the maximum contour length to lower values.

Assume that the contour length $(p-1)a$ of the fragment defined by \mathbf{x}_f of the above molecules corresponds to the adaptive length scale at strain ϵ_1 . Then, at strain $\epsilon_2 > \epsilon_1$, the configurational distribution function, $\psi_f(\mathbf{x}_f|Q_f,Q,t)$ may deviate from the corresponding equilibrium distribution function by a greater extent because the configuration of the molecules has been distorted further by the flow. In this case the inverse Langevin function no longer applies over the length $(p-1)a$, and the adaptive length scale decreases further.

Next consider the evolution of the adaptive length scale at large strains where the molecules become increasingly unraveled until almost all have an end-to-end distance near the maximum contour length. There exists a subset of Kramers chains with *end-to-end distance Q_c close to Q_0* whose internal configurations are described by the distribution function $\psi(\mathbf{x}|Q_c,t)$. Such molecules have a rodlike shape and have a configuration

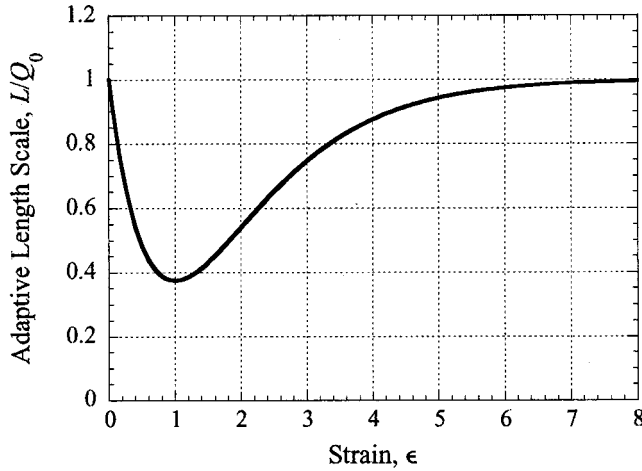


FIG. 2. Qualitative evolution of the adaptive length scale L with strain for a rapid, uniaxial extensional flow. The adaptive length is scaled by the contour length of the complete molecule Q_0 .

space that is a narrow tube surrounding the molecule. Since the configuration space is so small, the molecules are able to sample it on a time scale much smaller than λ_d despite the presence of a strong underlying flow. Consequently, $\psi(\mathbf{x}|Q_c, t)$ does not deviate much from the corresponding equilibrium distribution function and the inverse Langevin function approximates well the end-to-end force of the entire molecule. Hence, the adaptive length scale approaches the maximum contour length.

Finally, we consider the evolution of the adaptive length scale averaged over an ensemble of molecules that represents the polymer solution. At $\epsilon = 0$, the average adaptive length scale is Q_0 for a quiescent fluid. For small strains, the ensemble-average adaptive length scale decreases, because most of the molecules have end-to-end distances close to the equilibrium value, and the adaptive length scale of such molecules decreases with increasing strain. However, at large strains the ensemble-averaged adaptive length scale increases and approaches Q_0 as the majority of molecules become almost fully extended, and the adaptive length scale of such molecules is close to Q_0 . The evolution of the ensemble-averaged adaptive length scale in the start-up of rapid uniaxial elongation is summarized schematically in Fig. 2. For elongation at small strain rates, the average adaptive length scale does not deviate very much from Q_0 at any strain, because the configurational distribution function $\psi(\mathbf{x}|Q, t)$ deviates little from its equilibrium value for any value of Q .

In the remainder of this section, we develop equations that describe the adaptive length scale in the limit that instantaneous changes in the flow field lead to instantaneous changes in the molecular parameters. The quantities so derived are denoted with an asterisk to signify this idealization; for example, the adaptive length scale in this limit is denoted by L^* . The fact that a molecule requires a finite time to react to a sudden change in the flow is incorporated in Sec. IV. The asterisk is dropped for the quantities calculated with this correction, so that the adaptive length scale following the correction is denoted by L .

Since the adaptive length scale L^* is the largest length scale for which the inverse Langevin function (or FENE force law approximation) applies, we model the polymer as a set of segments, each represented by a FENE spring whose maximum length equals L^* . The force law of a segment with a maximum length of L^* is given by

$$F_{\text{seg}}^{*(s)} = \frac{H_{\text{seg}}^* Q}{1 - (Q^2/L^*{}^2)}. \quad (19)$$

In order for the model always to represent a polymer of the same maximum contour length, the number of segments is set to equal the contour length of the entire molecule divided by L^* or

$$M_{\text{seg}}^* = \frac{(N-1)a}{L^*}. \quad (20)$$

Equation (20) allows the existence of a fractional number of segments. The number of beads also can be fractional and is defined to be one greater than the number of segments

$$N_{\text{bead}}^* = M_{\text{seg}}^* + 1. \quad (21)$$

In order to minimize the complexity of the model, we assume that *the orientations and lengths of all segments are identical*. Without this assumption, it would be necessary to know how to map two FENE spring chains with different numbers of springs onto one another. As discussed above, we choose to avoid this problem.

The spring constant and the drag coefficient are functions of the number of segments. As the number of segments increases, each segment represents a smaller number of links of the Kramers chain. The spring constant H_{seg}^* is inversely proportional to the number of links in a segment and is thus proportional to the number of segments

$$H_{\text{seg}}^* = \frac{3M_{\text{seg}}^* kT}{(N-1)a^2}. \quad (22)$$

As the number of segments increases, each segment represents a smaller fragment of the polymer, and, therefore, the drag on each of the beads attached to the segment decreases according to

$$\lambda_{\text{seg}}^* = \frac{\zeta_{\text{seg}}^*}{4H_{\text{seg}}^*} = \frac{\lambda_d}{K^*}, \quad (23)$$

where

$$K^* = \left(\frac{b_{\text{seg}}^*}{b_{\text{seg}}^* + 5} \right) \left(\frac{\sqrt{(b_{\text{max}} + 5)(b_{\text{max}} + 7)}}{b_{\text{max}}} \right) \left\{ \frac{[2(M_{\text{seg}}^* + 1)^2 + 7][(M_{\text{seg}}^* + 1)^2 - 1]}{45} \right. \\ \left. - \frac{12[(M_{\text{seg}}^* + 1)^2 + 1][(M_{\text{seg}}^* + 1)^2 - 1]}{45(M_{\text{seg}}^* + 1)(b_{\text{seg}}^* + 7)} \right\}^{1/2}. \quad (24)$$

Equation (23) is similar to Eq. (17) because we assume the time constant of a segment $\lambda_{\text{seg}}^* = \zeta_{\text{seg}}^*/4H_{\text{seg}}^*$ scales with the longest relaxation time of the polymer $\lambda_d = \zeta_d/4H_d$ in the same way that the time constant λ_s of a spring in a FENE chain scales with λ_d . The parameter b_{seg}^* is the dimensionless finite extensibility parameter for a segment with maximum extension equal to the adaptive length scale L^* and is defined as

$$b_{\text{seg}}^* = \frac{H_{\text{seg}}^* L^*{}^2}{kT}. \quad (25)$$

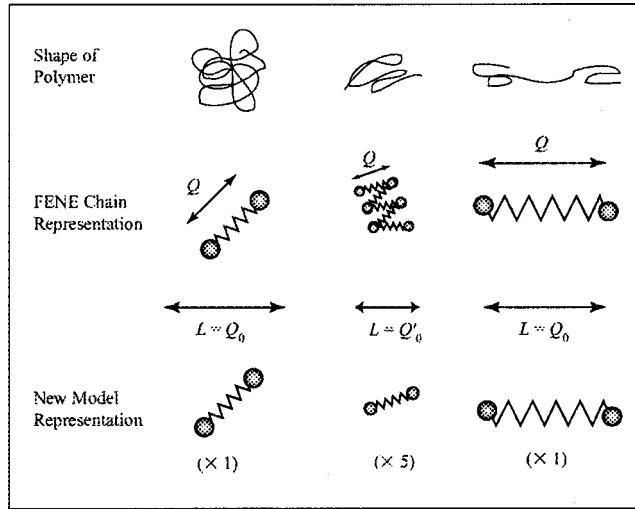


FIG. 3. ALS model representations of an equilibrium coil, a polymer stretched to small strains in a rapid extensional flow, and a fully stretched polymer. Here L is the adaptive length scale, Q_0 is the maximum length of the molecule, and Q'_0 is the maximum length of a segment.

Substituting Eqs. (20) and (22) into Eq. (25) yields a relationship between b_{seg}^* and M_{seg}^* as

$$b_{\text{seg}}^* M_{\text{seg}}^* = 3(N-1) = b_{\max}. \quad (26)$$

Since the middle term of Eq. (26) equals the value that the finite extensibility parameter b_{seg}^* would take if the polymer were represented by a single FENE spring (or FENE dumbbell), we denote it as b_{\max} .

The relationship between the adaptive length scale and the number of segments is illustrated in Fig. 3. Here some characteristic configurations of a polymer molecule, such as an equilibrium coil, a polymer molecule stretched to small strains in a rapid extensional flow, and a fully stretched polymer, are represented by a FENE model and by the ALS model. The FENE dumbbell represents well the equilibrium coil and fully stretched polymer. Similarly, the ALS model represents both of these conformations by a single segment with the adaptive length scale equal to Q_0 . In contrast, the ALS model represents the kinked conformation by several identical segments, each with a maximum extension given by the adaptive length scale. The adaptive length scale equals Q_0 divided by the number of segments.

Having defined and developed a qualitative understanding for the adaptive length scale, it remains to propose an equation for it. To do this, we assert that a fragment of a polymer chain can sample its configuration space if the time constant for the fragment is similar in magnitude to the time scale of the underlying flow. Near equilibrium, the relaxation time scale of a spring is $\lambda_{\text{seg}}^* = \zeta_{\text{seg}}^*/4H_{\text{seg}}^*$. However, when the segment stretches close to its maximum extension, the relaxation time scale of the spring decreases because the spring modulus stiffens as $[1 - (Q^2/L^{\ast 2})]^{-1}$. For steady uniaxial extension, the time scale of the flow is $\dot{\epsilon}^{-1}$. Equating these time scales yields

$$\frac{Z}{\dot{\epsilon}} = \frac{\zeta_{\text{seg}}^*}{4H_{\text{seg}}^* \sqrt{\left(1 - \frac{\hat{Q}^2}{L^{*2}}\right)}}. \quad (27)$$

The time constants of the flow and of the segment of the molecule are required to be similar in Eq. (27), but not identical. That is, Z should be an order one constant, but its precise value is not set by the theory. If a value less than unity is chosen, then the adaptive length scale L^* decreases for given flow conditions, and this will lead to even more rapid growth in the extensional stress. On the other hand, the FENE dumbbell model can be conveniently recovered from the ALS model by letting $Z \rightarrow \infty$.

In the remainder of this paper, equations are expressed in dimensionless form by making time dimensionless with the longest time constant of the molecule λ_d and by making length dimensionless with $\sqrt{kT/H_d}$. The spring constant H_d is that for a dumbbell representing the entire molecule and is defined by Eq. (10) with $M = 1$. All dimensionless quantities are henceforth denoted with the symbol \wedge . In the process of making the equations dimensionless, the ratio H_{seg}^*/H_d frequently appears. By dividing Eq. (22) by Eq. (10) with M set to unity, this ratio can be written as

$$\frac{H_{\text{seg}}^*}{H_d} = M_{\text{seg}}^*. \quad (28)$$

By using Eq. (28) and recalling that M_{seg}^* and b_{seg}^* are inversely related through Eq. (26), Eq. (27) is written in dimensionless form as a nonlinear equation in b_{seg}^* :

$$\frac{\text{Wi}}{K^*} \left(1 - \frac{\hat{Q}^2}{b_{\text{seg}}^*} \frac{b_{\text{max}}}{b_{\text{seg}}^*} \right) = Z, \quad (29)$$

where

$$\text{Wi} = \lambda_d \dot{\epsilon}. \quad (30)$$

We define b_{seg}^* to have a piecewise description such that it equals the value given by Eq. (29) if that value is less than b_{max} . Otherwise, b_{seg}^* is set to b_{max} . Once b_{seg}^* has been calculated, the number of segments M_{seg}^* is easily found by using Eq. (26). Finally, the adaptive length scale L^* is obtained by substituting M_{seg}^* into Eq. (20).

Figure 4 shows the relation between M_{seg}^* and \hat{Q}^2 for a variety of Weissenberg numbers as given by Eq. (29). For $\text{Wi} < 1$, M_{seg}^* is equal to unity for all values of \hat{Q}^2 . This is because at low Wi a polymer chain is stretched reversibly, and the FENE force law is valid for the overall chain. For $\text{Wi} > 1$, M_{seg}^* is greater than unity for low values of \hat{Q}^2 . This reflects the fact that at low strains, when the molecules have still not unraveled, the time constant of the flow is equal to the time constant of only a small fragment of the polymer. Hence the adaptive length scale is small, and the number of segments is greater than unity. As \hat{Q} approaches the maximum contour length of the molecule, the time constant of the molecule decreases and approaches the time constant of the flow. Consequently, the adaptive length scale tends to the maximum contour length, and a single segment may represent the entire molecule. Thus, the criterion in Eq. (27) correctly represents all the aspects of polymer chain behavior that seem to be important in strong elongational flows.

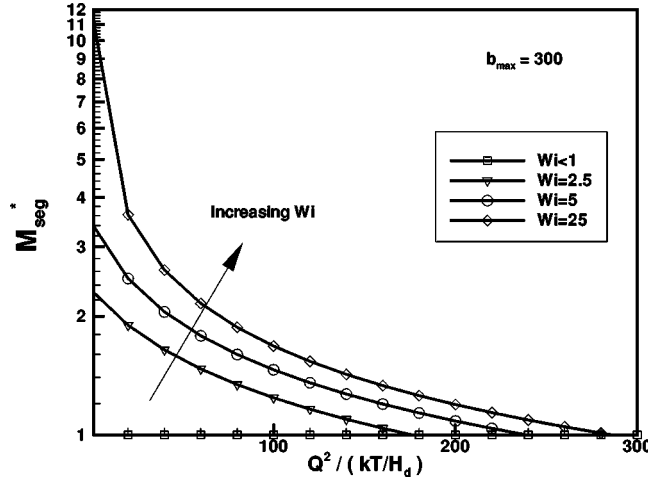


FIG. 4. The dependence of M_{seg}^* on \dot{Q}^2 in elongational flow for various Wi .

In order to generalize Eq. (27) for an arbitrary flow, the elongation rate $\dot{\epsilon}$ must be replaced by a more general quantity $\dot{\epsilon}_g$ that measures the local deformation rate in the vicinity of the polymer chain. The transpose of the velocity gradient tensor $\boldsymbol{\kappa}$ can be decomposed into the rate-of-strain tensor $\dot{\gamma}$, which describes the rate-of-deformation of a fluid element (and, therefore, the polymer contained within it), and the vorticity $\boldsymbol{\omega}$, which describes the rigid rotation of the fluid element. The direction of the principal axis of the deformation-rate tensor is given by the eigenvector \mathbf{n} , which corresponds to the largest absolute eigenvalue of $\dot{\gamma}$. In accordance with Tanner (1976) and Olbricht *et al.* (1982), we choose $\dot{\epsilon}_g$ to be the maximum absolute eigenvalue of the rate-of-strain tensor $\dot{\gamma}$ as indicated by

$$\dot{\epsilon}_g = \frac{1}{2} |\max[\text{Eig}(\dot{\gamma})]|. \quad (31)$$

For uniaxial elongational flow, $\dot{\epsilon}_g$ simply reduces to the elongation rate.

It is important to note that the parameters of the ALS model can be derived solely from knowledge of two molecular properties (the molecular weight and characteristic ratio of the polymer) and from measurement of the ratio of the zero-shear-rate first normal stress coefficient to the zero-shear-rate polymer contribution to viscosity. From the molecular weight and characteristic ratio, the number of rods N in the equivalent Kramers chain can be calculated by using Eq. (1). Substituting N into Eq. (26) yields the value of b_{max} , and the number of segments M_{seg}^* can be expressed as $b_{\text{max}}/b_{\text{seg}}^*$. The time constant of the polymer is determined from the ratio of the zero-shear-rate first normal stress coefficient to the zero-shear-rate polymer contribution to viscosity in Eq. (3). Once the flow kinematics are given, the dimensionless adaptive length b_{seg}^* in the ALS model can be determined by solving Eq. (29).

IV. EVOLUTION EQUATION FOR THE ADAPTIVE LENGTH SCALE

In the development in Sec. III, the adaptive length scale L^* and the other asterisked quantities have been assumed to adjust instantaneously to changes in the flow. However, such instantaneous changes in L^* lead to instantaneous changes in the number of segments and, therefore, to “jumps” in the polymer contribution to the stress. For flexible

polymers, there have been no conclusive experimental observations of jumps in the polymer contribution to the stress upon the sudden inception of a flow. Additionally, it has been argued earlier in this paper that instantaneous jumps in the adaptive length scale do not occur. Instead, the adaptive length scale L^* as derived from Eq. (29), should be thought of as a pseudosteady state value that the system tends toward, but which is not reached instantaneously. In the rest of this section, relations are developed to describe the behavior of microstructural properties, without the approximation that molecular changes occur instantaneously upon a sudden change in flow. The absence of this approximation is reflected in our notation by the removal of the asterisks.

The first task is to develop an evolution equation for the adaptive length scale L that describes its approach to L^* . We emphasize that our approach is not a rigorous derivation in a kinetic theory framework. However, our evolution equation is fundamentally motivated by simulations of Kramers chain behavior. The evolution equation should have a stiffening term that causes L to decrease towards L^* when the flow is initiated and a relaxation term that makes the adaptive length scale return to Q_0 when the flow is stopped. We propose that the relaxation of the segment be proportional to the difference between L and Q_0 and occur on a time scale equal to $\lambda_{\text{seg}} = \zeta_{\text{seg}}/4H_{\text{seg}}$, which varies as the relaxation occurs. This gives the following description of the relaxation process

$$\left(\frac{dL}{dt}\right)_{\text{relax}} = \frac{(Q_0 - L)}{\lambda_{\text{seg}}} = \frac{(Q_0 - L)}{\lambda_d/K}, \quad (32)$$

where the expressions for H_{seg} , K , L , and Q_0 are given by Eqs. (22), (24), (25), and (12), respectively, except that the asterisks are removed from all quantities.

The stiffening term deserves more detailed consideration. First, Rallison (1996) showed that in a uniaxial elongational flow, the rate at which a molecule is compressed into a one-dimensional structure that can exhibit kinks is proportional to Wi . The segments of the ALS model crudely represent these kinks. This kink formation is expected to decrease as the segment stretches close to its maximum extension. In shear flow, the stiffening is also associated with the finite extensibility parameter. Since the value of shear rate for the onset of shear thinning in the viscosity is proportional to Q_0 and thus $b_{\max}^{1/2}$ [Bird *et al.* (1987)], the stiffening in shear flow is inversely proportional to $b_{\max}^{1/2}$. Hence, for an arbitrary flow, we propose that the stiffening is proportional to Wi^{eff} , which is defined as

$$\text{Wi}^{\text{eff}} = \lambda_d \dot{\epsilon}^{\text{eff}} = \frac{1}{2} \lambda_d \max[\text{Eig}(\dot{\gamma}^{\text{eff}})], \quad (33)$$

where

$$\dot{\gamma}^{\text{eff}} = \begin{pmatrix} 2\kappa_{11} & s(\kappa_{21} + \kappa_{12}) \\ s(\kappa_{21} + \kappa_{12}) & 2\kappa_{22} \end{pmatrix}; \quad s = (b_0/b_{\max})^{1/2} \quad (34)$$

and b_0 is a fitting parameter that governs the onset of shear thinning behavior. The components of the transpose of the velocity gradient tensor $\boldsymbol{\kappa}$ are expressed in Protean coordinates [Adachi (1983)] in which basis vectors are the unit tangent and unit normal vectors to the streamlines for a two-dimensional flow.

Second, the evolution of the configuration of a particular polymer molecule depends on its initial conformation. Thus, the evolution equation for the adaptive length scale should reflect this, since the adaptive length scale is closely related to the conformation a molecule assumes. Larson *et al.* (1999) examined the influence of initial configuration on the configurational evolution of wormlike chains in a planar elongational flow. They

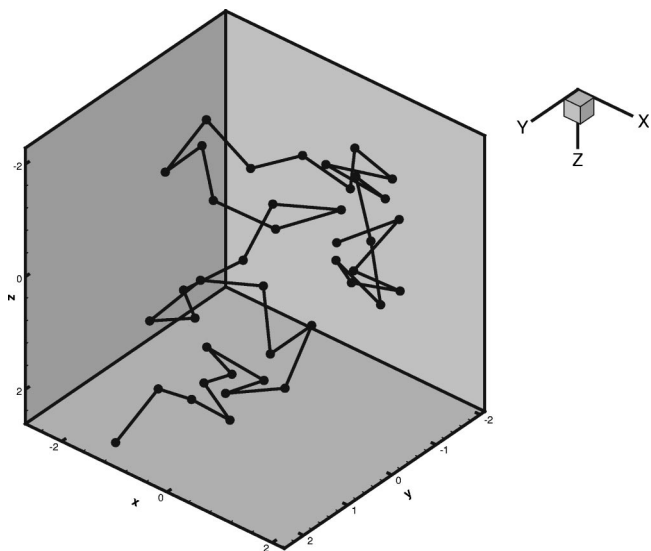


FIG. 5. Configuration of the “dumbbell prone” polymer used to study the effects of initial configuration on subsequent stress growth in a uniaxial extensional flow.

noted that polymers whose end-to-end vectors lie initially in the plane of stretching unravel rapidly to their maximum extension. However, molecules that are initially oriented perpendicular to the flow direction stretch out much more slowly and display a prominent knee in plots of extension versus strain. We have performed a similar analysis for uniaxial elongational flow. We also investigate the dependence of stress growth on the initial end-to-end orientation of the macromolecule with respect to the flow direction and model this dependence through the stiffening term of the evolution equation for the adaptive length scale.

The relationship between the initial end-to-end orientation and stress growth is analyzed by using a 40-link Kramers chain selected from an ensemble of Kramers chains at equilibrium whose terminal beads are at opposite extremities of the polymer coil. The configuration of the polymer, which is shown in Fig. 5, is dumbbell-prone according to the terminology of Larson *et al.* (1999). This Kramers chain is subjected to startup of steady uniaxial elongational flow with the principal direction of stretching parallel to the initial end-to-end vector. A total of 1000 trajectories are computed with the chain starting from the same initial configuration, but experiencing different sequences of random numbers. Finally, the ensemble-averaged stress and end-to-end distance are calculated as functions of strain. The effect of initial orientation is investigated by repeating the calculations with the initial configuration of the Kramers chain rotated by an increment of 10° further away from the axis of elongation in each set of calculations.

Figures 6 and 7 show the evolution of the end-to-end distance and stress for molecules that are initially oriented 0° , 20° , 40° , 50° , 70° , and 90° to the principal axis of elongation. The end-to-end distance and stress increase most rapidly for the molecules that are initially aligned parallel to the flow and most slowly for the molecules that are initially perpendicularly aligned. The rates of growth of stress and end-to-end distance decrease monotonically with increase of the initial angle made by the molecule with the principal stretching direction. The decreases in rates of growth of stress and end-to-end distance are particularly dramatic as this initial angle is increased from 40° to 50° . This prediction

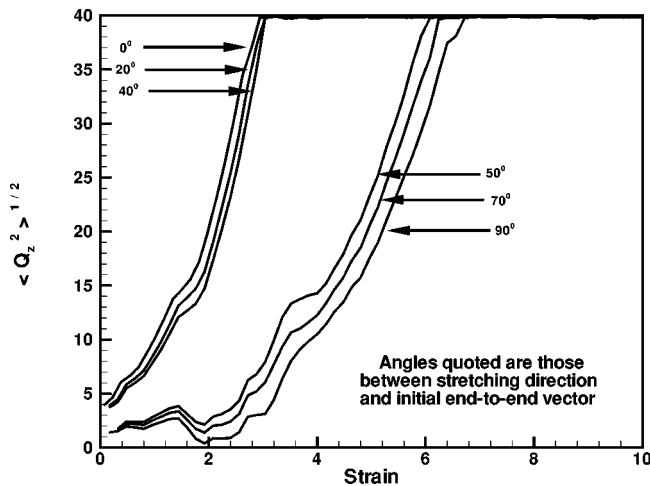


FIG. 6. Effect of initial orientation on the evolution of the z component of the end-to-end distance of polymer molecules in startup of steady uniaxial elongational flow at $Wi = 45.6$.

is consistent with the results of Larson *et al.* (1999) who show that a molecule becomes “kink prone” rather than “dumbbell prone” as its end-to-end vector is rotated away from the stretching direction.

The calculation is repeated for an equivalent FENE dumbbell ($b = 120$) with initial end-to-end vector equal to that of the Kramers chain. Figure 8 shows that the FENE dumbbell that is initially aligned parallel to the stretching direction adequately describes the stress growth of the Kramers chain. However, the FENE dumbbell initially aligned perpendicular to the flow direction greatly underpredicts the stress of the corresponding Kramers chain up to $\epsilon = 5$. It appears that the inability of the FENE dumbbell to describe the stress growth of the Kramers chain at low strains is due largely to the dumbbells that are initially aligned perpendicular to the flow. This is because molecules that are

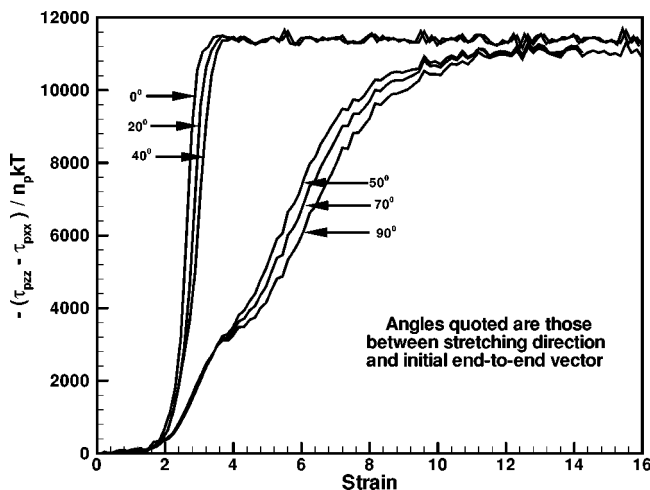


FIG. 7. Effect of initial orientation on stress growth in startup of steady uniaxial elongational flow at $Wi = 45.6$.

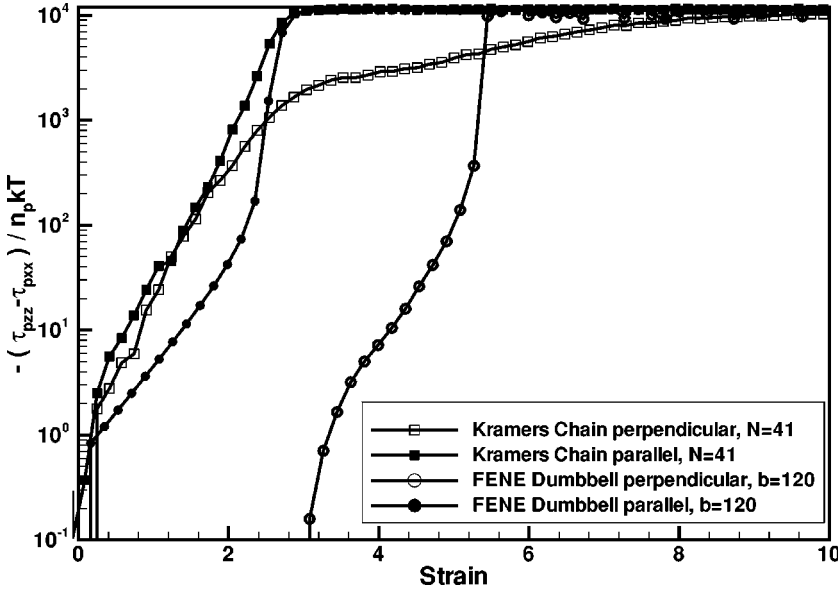


FIG. 8. Comparison of the effect of initial orientation on stress growth in polymer molecules represented by Kramers chains and FENE dumbbells in startup of steady uniaxial elongational flow at $\text{Wi} = 45.6$.

initially aligned perpendicular to the flow evolve into kinked structures whose adaptive length scale is less than Q_{0d} , where Q_{0d} is the maximum length of the entire polymer molecule. It is for these molecules that the adaptive length scale has to evolve towards L^* .

In summary, studies of Rallison (1996) show that the rate of molecular stiffening is proportional to the Weissenberg number of the flow. The stiffening process, which is represented by allowing L to tend towards L^* , decreases as the segment stretches close to its maximum extension. We propose that this process occurs on a time scale of the segment equal to $\lambda_{\text{seg}}^* = \zeta_{\text{seg}}^*/4H_{\text{seg}}^*$. Finally, the rate of the stiffening increases with the angle the molecule makes with the stretching direction. Based on these observations, we propose a stiffening term in the evolution equation for L of the form

$$\begin{aligned} \left(\frac{dL}{dt} \right)_{\text{stiffen}} &= - \left| \mathbf{n} \times \frac{\mathbf{Q}}{|\mathbf{Q}|} \right| \frac{\text{Wi}^{\text{eff}} [1 - (Q^2/L^{*2})](L - L^*)}{\lambda_{\text{seg}}^*} \\ &= - \left| \mathbf{n} \times \frac{\mathbf{Q}}{|\mathbf{Q}|} \right| \frac{\text{Wi}^{\text{eff}} [1 - (Q^2/L^{*2})](L - L^*)}{\lambda_d/K^*}, \end{aligned} \quad (35)$$

where \mathbf{n} is the unit vector parallel to the eigenvector of the rate-of-strain tensor that corresponds to its largest eigenvalue.

Combining the relaxation and stiffening terms gives the evolution equation for the adaptive length in dimensionless form

$$\frac{db_{\text{seg}}}{d\hat{t}} = - \underbrace{\left| \mathbf{n} \times \frac{\hat{\mathbf{Q}}}{|\hat{\mathbf{Q}}|} \right| \text{Wi}^{\text{eff}} \left(1 - \frac{\hat{Q}^2}{b_{\text{seg}}^*} \frac{b_{\text{max}}}{b_{\text{seg}}^*} \right) (b_{\text{seg}} - b_{\text{seg}}^*) K^*}_{\text{stiffening}} + \underbrace{(b_{\text{max}} - b_{\text{seg}}) K}_{\text{relaxing}}. \quad (36)$$

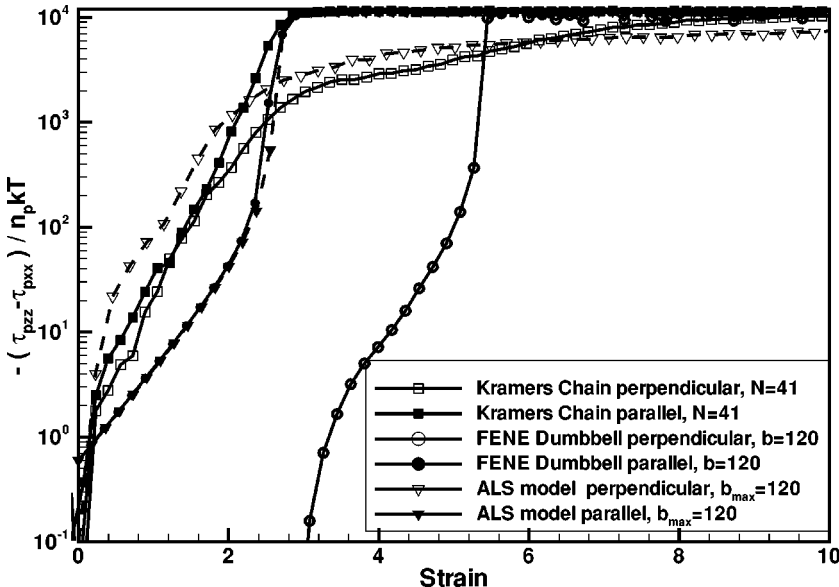


FIG. 9. Comparison of the effect of initial orientation on stress growth in the startup of steady uniaxial elongational flow for polymer molecules as represented by a Kramers chain, FENE dumbbell, and the ALS model at $\text{Wi} = 45.6$.

The terms K^* and K on the right-hand side of Eq. (36) are ratios of the longest relaxation time of the polymer (λ_d) to the time constants (λ^* and λ) of a single segment. After incorporating Eq. (36) into the new model, two realizations of the new model (one initially perpendicular and one initially parallel with the flow direction) are simulated in order to compare the dependence of stress growth upon initial orientation with the Kramers chain and FENE dumbbell. The results are shown in Fig. 9. Molecules initially aligned parallel to the stretching direction behave identically to the corresponding FENE dumbbell. However, the stress associated with the molecules initially aligned perpendicular to the stretching direction grows more quickly than that for the FENE dumbbell at low strains and behaves very similarly to the stress associated with the corresponding Kramers chain.

The reason for the better agreement of the ALS model with the Kramers chain is understood from Fig. 10, which shows the evolution of $\langle b_{\text{seg}} \rangle$ and $\langle b_{\text{seg}}^* \rangle$ in the startup of steady uniaxial elongational flow at $\text{Wi} = 11.4$ for the ALS model after the incorporation of Eq. (36). Here, $\langle b_{\text{seg}} \rangle$ and $\langle b_{\text{seg}}^* \rangle$ are ensemble averages of b_{seg} and b_{seg}^* , respectively, at a given strain. When the flow is started, $\langle b_{\text{seg}} \rangle$ decreases rapidly towards $\langle b_{\text{seg}}^* \rangle$. At $\epsilon = 1.0$, $\langle b_{\text{seg}} \rangle$ is still greater than $\langle b_{\text{seg}}^* \rangle$ but begins to increase towards b_{max} as the relaxation term in Eq. (36) begins to dominate the stiffening term. The increase in $\langle b_{\text{seg}} \rangle$ for $\epsilon > 1.0$ is also driven by the increase in $\langle b_{\text{seg}}^* \rangle$. The rise in $\langle b_{\text{seg}}^* \rangle$ is due to the increase in L^* at large strains due to the mechanisms described in Sec. III. Although Eq. (36) was derived from a consideration of uniaxial elongational flow, we propose that it can be generalized to arbitrary flows by defining the magnitude of the deformation rate by Eq. (33).

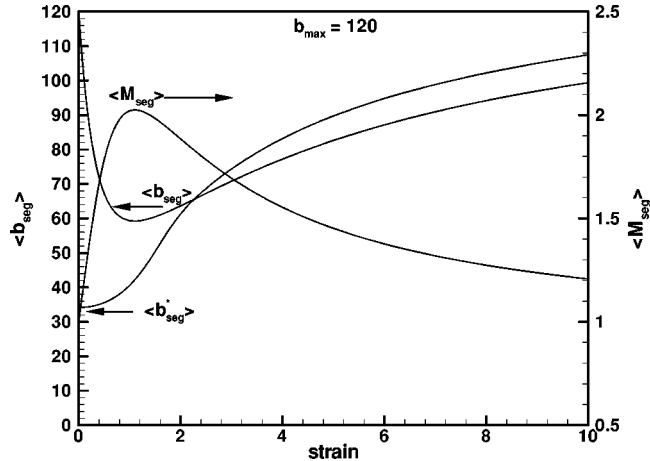


FIG. 10. Evolution of $\langle b_{\text{seg}}^* \rangle$, $\langle b_{\text{seg}} \rangle$, and $\langle M_{\text{seg}} \rangle$ for the ALS model for startup of steady uniaxial elongational flow at $Wi = 11.4$.

V. EQUATIONS OF MOTION, STRESS, AND BIREFRINGENCE FOR THE ALS MODEL

Assuming that the configurations of all segments are identical, it follows that the motion of each segment is described by the same stochastic differential equation. Thus the dynamical equation for the motion for the ALS model is similar to that for a FENE dumbbell except that the drag coefficient, the spring constant, and the maximum extensibility of the spring all vary with the number of segments, where the drag coefficient of a bead attached to this segment is related to the drag on a bead in a FENE dumbbell according to Eq. (23) (with the asterisks removed from the quantities). This formulation assumes that the time constant of a segment is related to the longest relaxation time of the molecule in the same way that the time constant of a spring in the FENE chain is related to the longest relaxation time of the chain. Hence, the dynamical equation for the motion for the ALS model is written in dimensionless form as

$$d\hat{\mathbf{Q}} = \left[Wi[\hat{\mathbf{k}} \cdot \hat{\mathbf{Q}}] - \frac{1}{2} K \left[\frac{\hat{\mathbf{Q}}}{1 - \frac{\hat{\mathbf{Q}}^2}{b_{\text{seg}}^2} \left(\frac{b_{\text{max}}}{b_{\text{seg}}} \right)} \right] d\hat{t} + \left(K \frac{b_{\text{seg}}}{b_{\text{max}}} \right)^{1/2} d\hat{\mathbf{W}}, \quad (37)$$

where K is given by Eq. (24) with the asterisks removed, and the evolution of b_{seg} is governed by Eqs. (29) and (36).

The polymer contribution to the stress for the ALS model is derived in a manner similar to that presented for the general dumbbell in Chapter 12 of Bird *et al.* (1987). However, whereas there is only one spring in a classical dumbbell, the ALS model may have several segments. Therefore, the stress contribution of one segment must be multiplied by the number of segments to give the contribution of the macromolecules to the stress. If the polymer contribution to the stress is made dimensionless by $n_p kT$, then the total polymeric stress is expressed in dimensionless form as

$$\hat{\tau}_p = \left\langle \frac{b_{\max}}{b_{\text{seg}}} \right\rangle \boldsymbol{\delta} - \left\langle \frac{(b_{\max}/b_{\text{seg}})^2 \hat{\mathbf{Q}} \hat{\mathbf{Q}}}{\left[1 - \frac{\hat{Q}^2}{b_{\text{seg}}} \left(\frac{b_{\max}}{b_{\text{seg}}} \right) \right]} \right\rangle. \quad (38)$$

The contribution to the birefringence from a single segment of the ALS model is identical to that for a FENE dumbbell and is obtained by setting M equal to unity in Eq. (16) and recognizing that the maximum extension of a segment is given by L . The total birefringence predicted by the ALS model is found by multiplying the birefringence from one segment by the number of segments. A segment of maximum extension L corresponds to n_s rods in the Kramers chain representation of the polymer; hence, n_s is equal to $(N-1)/M_{\text{seg}}$. To generate a dimensionless expression for birefringence, the end-to-end vector is again made dimensionless with the characteristic length, $\sqrt{kT/H_d}$. The characteristic length is written as $(N-1)a^2/3$ by substituting for H_d from Eq. (10) with M set to unity. Recalling that L is given by $(N-1)a^2/M_{\text{seg}}$ and substituting for n_s gives the dimensionless expression for the birefringence of the ALS model as

$$\Delta n = \frac{5}{3} C n_p k T \left\langle \left(\frac{b_{\max}}{b_{\text{seg}}} \right)^2 (\hat{Q}_z \hat{Q}_z - \hat{Q}_x \hat{Q}_x) \right\rangle, \quad (39)$$

where C is given by Eq. (8).

VI. BEHAVIOR OF THE ALS MODEL AT LOW DEFORMATION RATES

Since the FENE spring force is applicable if a polymer is slowly stretched, it is important to demonstrate that the ALS model reduces to the FENE dumbbell in the limit of low deformation rates. As shown in Fig. 4, the value of b_{seg} is equal to b_{\max} for all Q^2 when $\text{Wi} < 1$. Additionally, if a polymer molecule has not been subjected to flow stronger than $\text{Wi} = O(1)$ in its recent flow history, then b_{seg} is also equal to b_{\max} . In this limit, both terms on the right-hand side of Eq. (36) are zero, and b_{seg} remains equal to b_{\max} . When b_{seg} equals b_{\max} , the ALS model behaves identically to the FENE dumbbell. Therefore, the ALS model exhibits the same behavior as the FENE dumbbell in weak flows.

Since the ALS model reduces to the FENE dumbbell model for low Weissenberg numbers, it duplicates an important success of the FENE dumbbell, which is to capture the universal stress-birefringence relaxation behavior of fully stretched Kramers chains [Doyle *et al.* (1998b)]. The new model represents a fully stretched chain as a single segment whose extensibility parameter b_{seg} is equal to b_{\max} . If the chains are allowed to relax in a quiescent solvent, the zero deformation rate renders b_{seg}^* equal to b_{\max} through Eq. (27), and both terms on the right-hand side of Eq. (36) equal zero. Therefore, b_{seg}^* is constant and equal to b_{\max} during the entire relaxation process, ensuring that the new model exhibits the universal stress-birefringence curve generated by the FENE dumbbell and Kramers chain.

VII. RHEOLOGICAL PREDICTIONS OF THE ALS MODEL

The mathematical formulation of the ALS model is now used to predict its rheological properties in simple shear and elongational flows. Results for steady and transient flows are presented in this section.

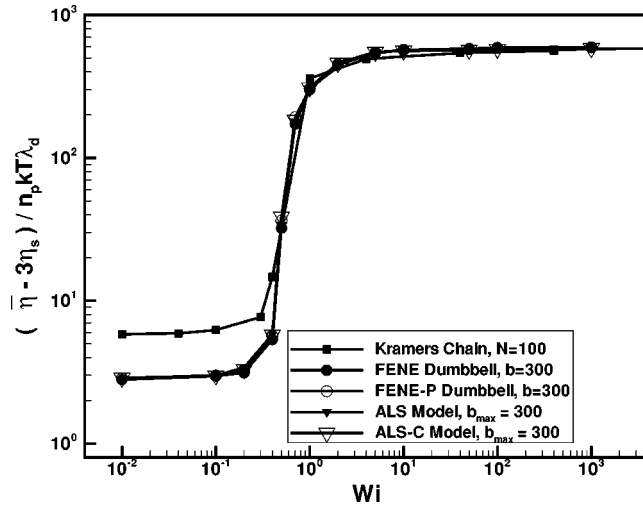


FIG. 11. Dependence of elongational viscosity on Wi for a 100-rod Kramers chain and the equivalent forms of the FENE dumbbell and ALS model. The results of the FENE-P dumbbell and ALS-C models are also shown.

A. Steady state elongational properties

In steady uniaxial elongational flow, polymer molecules are fully unraveled into rod-like structures at Weissenberg numbers large enough to induce the coil-stretch transition. In the unraveled state, the adaptive length scale of the ALS model equals the maximum extension of the molecule. Consequently, b_{seg} is equal to its maximum value b_{max} and the ALS model predicts the same elongational viscosity as the FENE dumbbell. This is confirmed in Fig. 11, which illustrates the dependence of the elongational viscosity on Wi for a 100-link Kramers chain, the equivalent FENE dumbbell, and the equivalent form of the ALS model. The data for the Kramers chain are taken from Doyle *et al.* (1997).

All three models have the identical elongational viscosity for $\text{Wi} \gg 1$. Each exhibits the coil-stretch transition at $\text{Wi} \approx 0.5$. The only difference among the predictions is that the Kramers chain has a higher elongational viscosity than the FENE dumbbell or the ALS model at values of Wi below the coil-stretch transition. This disagreement among the models for $\text{Wi} \ll 1$ arises because, as shown by Doyle *et al.* (1997), the Kramers chain and the FENE dumbbell cannot predict the same values for the following pairs of properties if the FENE dumbbell has a constant drag coefficient: (a) the steady-state elongational viscosity at zero and infinite elongation rates and (b) the zero-shear-rate viscosity and zero-shear-rate first normal stress coefficient. Doyle *et al.* (1997) chose the bead drag coefficient for the FENE dumbbell to be $(2/3)N\zeta$ in order to match the zero-shear-rate viscosity of the Kramers chain. With this choice, the FENE dumbbell predicts the zero-shear-rate first normal stress coefficient to be twice that of the Kramers chain. Additionally, the FENE dumbbell predicts the same elongational viscosity as the Kramers chain at low Wi . However, for $\text{Wi} \gg 1$, the steady-state elongational viscosity is twice the value given by the Kramers chain.

Our analysis is primarily concerned with comparing the models for representations of molecules far from equilibrium. Therefore, the drag coefficient of a bead for the FENE dumbbell is related to the drag on the bead of a Kramers chain by assuming that the longest relaxation times of the Kramers chain and FENE dumbbell are identical and given by Eq. (4). This method of relating the drag coefficient results in matching the elongational viscosities of the Kramers chain and FENE dumbbell in the limit Wi

$\rightarrow \infty$, as shown below. Liu (1989) notes that the polymer contribution to the zero-shear-rate viscosity of a Kramers chain is given by

$$(\eta_0 - \eta_s) = \frac{1}{36} n_p \zeta a^2 (N^2 - 1). \quad (40)$$

Rewriting ζ in terms of λ_d by using Eq. (4) gives the zero-shear-rate viscosity for $N \gg 1$ as

$$(\eta_0 - \eta_s) = 1.956 n_p k T \lambda_d. \quad (41)$$

This result demonstrates that the Kramers chain predicts approximately twice the polymer contribution to the zero-shear-rate viscosity as the FENE dumbbell. Furthermore, Liu also notes that the elongational viscosity in the limit of very high extension rates is

$$\lim_{\dot{\epsilon} \rightarrow \infty} \left[\frac{\bar{\eta} - 3 \eta_s}{3(\eta_0 - \eta_s)} \right] = N. \quad (42)$$

By substituting for $\eta_0 - \eta_s$ according to Eq. (41), Eq. (42) is rewritten as

$$\lim_{\dot{\epsilon} \rightarrow \infty} \left[\frac{\bar{\eta} - 3 \eta_s}{3n_p k T \lambda_d} \right] = 1.956 N, \quad (43)$$

which is very similar to the prediction for a FENE dumbbell given by Bird *et al.* (1987), namely,

$$\lim_{\dot{\epsilon} \rightarrow \infty} \left[\frac{\bar{\eta} - 3 \eta_s}{3n_p k T \lambda_d} \right] = 2 \left(\frac{b_{\max} + 3}{3} \right) \approx 2N. \quad (44)$$

Despite the agreement between the FENE dumbbell and Kramers chain models for $Wi \gg 1$, the choice of drag coefficient for the FENE dumbbell leads to different values of elongational viscosity for $Wi \ll 1$. This discrepancy is understood by analyzing the analytical results for the elongational viscosity in the limit of low elongation rates. For $\dot{\epsilon} \ll 1$, Hassager (1974) gives $\bar{\eta}(\dot{\epsilon})$ as

$$\frac{\bar{\eta} - 3 \eta_s}{3(\eta_0 - \eta_s)} \sim 1 + \frac{N^2 \zeta a^2 \dot{\epsilon}}{90kT}. \quad (45)$$

Rewriting ζ in terms of λ_d and substituting for $\eta_0 - \eta_s$ according to Eq. (41) gives

$$\frac{\bar{\eta} - 3 \eta_s}{n_p k T \lambda_d} \sim 5.87(1 + 0.782 Wi) \quad (Wi \rightarrow 0). \quad (46)$$

In contrast, Eqs. (13.5-45) of Bird *et al.* (1987) gives the elongational viscosity of the FENE dumbbell at low elongation rates as

$$\frac{\bar{\eta} - 3 \eta_s}{n_p k T \lambda_d} \sim \frac{3b_{\max}}{b_{\max} + 5} \left(1 + \frac{b_{\max}}{b_{\max} + 7} Wi \right) \quad (Wi \rightarrow 0). \quad (47)$$

This analysis explains why the elongational viscosity of the Kramers chain is twice that of the FENE dumbbell as $\dot{\epsilon} \rightarrow 0$ (Fig. 11).

B. Viscometric properties

Figures 12 and 13 show the dependence of the viscosity and first normal stress coefficient of a 100 link Kramers chain, the equivalent FENE dumbbell, and the equivalent

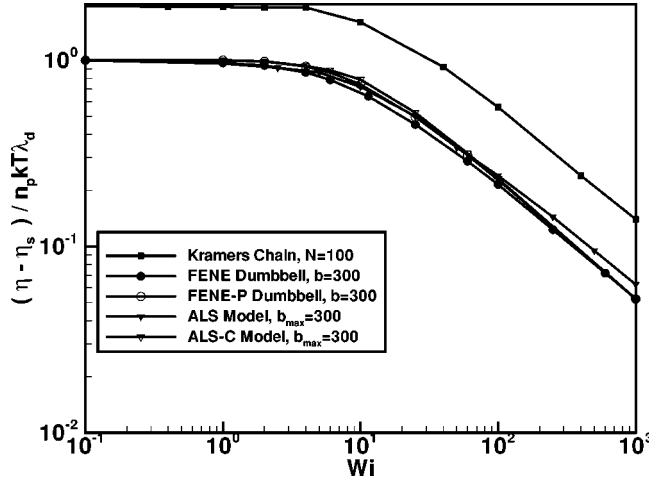


FIG. 12. Dependence of viscosity on Wi for a 100-rod Kramers chain and the equivalent forms of the FENE dumbbell, FENE-P dumbbell, ALS, and ALS-C models. The parameter b_0 in Eq. (34) is chosen to be 120.

form of the ALS model on Wi for steady shear flow. The results for the Kramers chain were obtained from Doyle *et al.* (1997).

The Kramers chain has twice the zero-shear-rate viscosity of the other two models. The zero-shear-rate viscosity of the FENE dumbbell is $n_p k T \lambda_d$, whereas η_0 for the Kramers chain is almost twice as large as shown by Eq. (41). The zero-shear-rate first normal stress coefficient $\Psi_{1,0}$ of the Kramers chain is about 1.5 times greater than that of the FENE dumbbell. For the FENE dumbbell, $\Psi_{1,0} = 2n_p k T \lambda_d^2$. By using Eq. (4) to replace λ_d in this expression, we find that $\Psi_{1,0} = 40328n_p \zeta^2 a^4/kT$ for a FENE dumbbell that represents a 100-link Kramers chain. On the other hand, by approximating $\Psi_{1,0}$ for the Kramers chain with the analytical result for a Fraenkel chain of infinitely stiff springs [Eqs. (16.5-13) of Bird *et al.* (1987)], the zero-shear-rate first normal stress co-

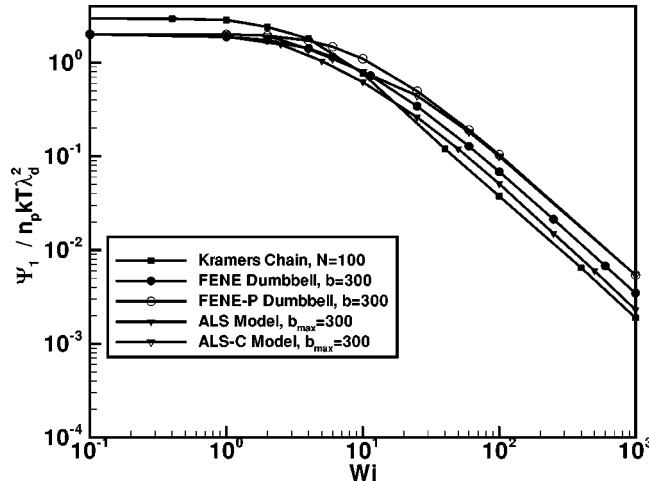


FIG. 13. Dependence of first normal stress coefficient on Wi for a 100-rod Kramers chain and the equivalent forms of the FENE dumbbell, FENE-P dumbbell, ALS, and ALS-C models. The parameter b_0 in Eq. (34) is chosen to be 120.

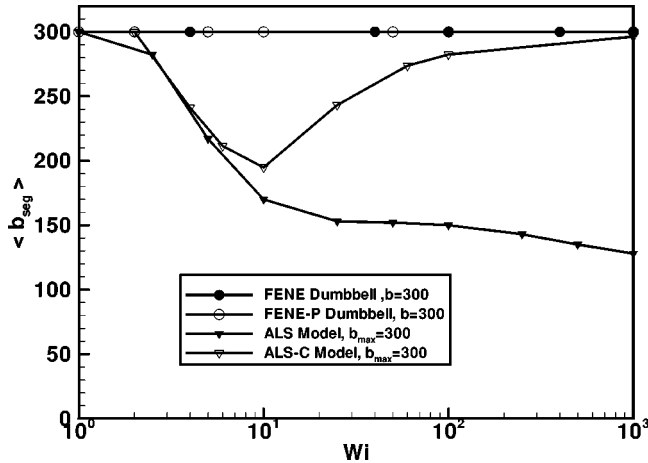


FIG. 14. Variation of $\langle b_{\text{seg}} \rangle$ with Wi in steady shear flow for the ALS and ALS-C models.

efficient of a Kramers chain is found to be $61003n_p\xi^2a^4/kT$. Hence, although the relation between the drag on a bead in a Kramers chain and a FENE dumbbell used in the ALS model results in the same $\bar{\eta}_\infty$ for the two models, it results in a mismatch in η_0 , $\Psi_{1,0}$, and $\bar{\eta}_0$.

Compared with the FENE dumbbell model, the onset of shear thinning in viscosity for the ALS model occurs at slightly larger Wi and the onset of shear thinning in first normal stress coefficient at slightly lower Wi .

The evolution of the internal configurational variable affects the shear flow properties of the new model in two important ways. First, as $\langle b_{\text{seg}} \rangle$ decreases in the ALS model, the contributions to the shear and normal stresses from a segment of the model are lower than if $\langle b_{\text{seg}} \rangle$ remained equal to b_{max} . This is because a segment with a reduced maximum extensibility a segment becomes fully stretched more readily. Once fully stretched, the segment rotates to align with the flow, thereby reducing its projected length perpendicular to the shearing direction. The decreased projected distance reduces the shear stress. A well known phenomenon that has a similar origin is that the onset of shear thinning in the FENE dumbbell model occurs at lower Wi for smaller values of b . Second, as $\langle b_{\text{seg}} \rangle$ decreases, $\langle M_{\text{seg}} \rangle$ increases, and this increases the stress contribution from the polymer molecules. Thus, a decrease in $\langle b_{\text{seg}} \rangle$ initiates two opposing effects. The relative magnitude of these effects determines the precise shear-flow response of the new model.

Figure 14 shows $\langle b_{\text{seg}} \rangle$ as a function of Wi for steady shear flow. The quantity $\langle b_{\text{seg}} \rangle$ decreases rapidly from 300 (or b_{max}) to 150 in the range of Wi of 1 to 100. For larger values of Wi , $\langle b_{\text{seg}} \rangle$ continues to decrease, though more slowly. The relationship of the shear flow properties as a function Wi to the behavior of the internal configurational variable can be understood in greater detail by examining the evolution of the distribution function for b_{seg} with Wi . As shown by Fig. 15, the distribution function for b_{seg} evolves from a delta function centered on b_{max} at $Wi < 1$ (not shown), to a more dispersed function centered on lower values of b_{seg} at larger Wi . At $Wi = 5$, the distribution function has an asymmetric inverted V shape. For $5 < Wi < 10$, the height of the inverted V decreases, the distribution function is shifted towards lower values of b_{seg} , and grows a progressively longer tail that extends to high values of b_{seg} . The shift of the distribution function is largely responsible for the reduction in $\langle b_{\text{seg}} \rangle$ in this range of Wi . The shift of the peak and the growth of the tail continue, and for larger Wi the distribution

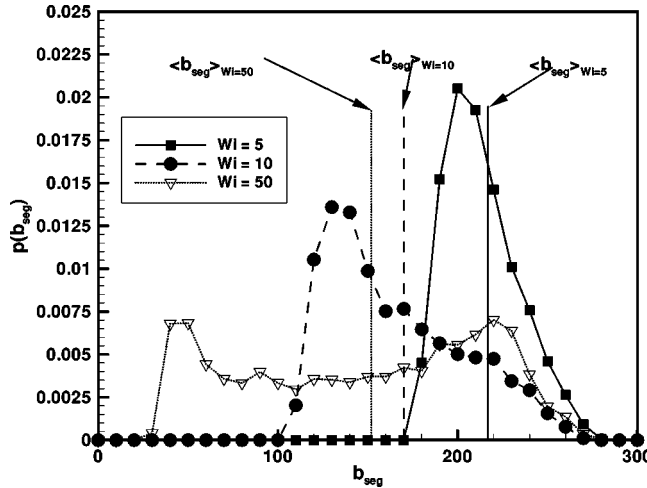


FIG. 15. Distribution function p of b_{seg} in steady shear flow for $\text{Wi} = 5, 10$, and 50 . The vertical lines indicate the average values $\langle b_{\text{seg}} \rangle$ corresponding to the three distribution functions shown.

function for b_{seg} converges to one that has an M shape. This implies that a polymer chain is in continuous tumbling-stretching motion at larger Wi , as predicted by Kramers chain simulations [Liu (1989)]. This prediction in steady shear flow has been experimentally verified by using video fluorescence microscopy [Smith *et al.* (1999)].

C. Start-up of steady uniaxial elongational flow

The normal stress difference ($\tau_{pzz} - \tau_{pxx}$) is displayed in Fig. 16 as a function of strain for a 40-link Kramers chain, the equivalent FENE dumbbell, and the equivalent ALS model in startup of steady uniaxial elongational flow. All three models give identical

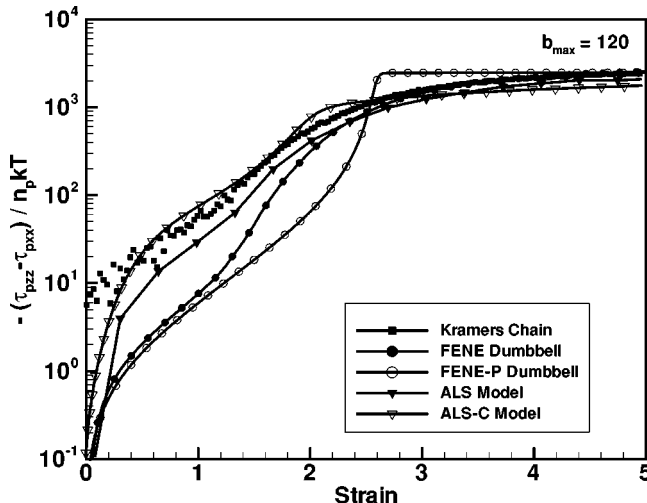


FIG. 16. Dependence of stress on strain for a 40-rod Kramers chain and the equivalent forms of the FENE dumbbell, FENE-P dumbbell, ALS, and ALS-C models in startup of steady uniaxial extensional flow at $\text{Wi} = 11.4$.

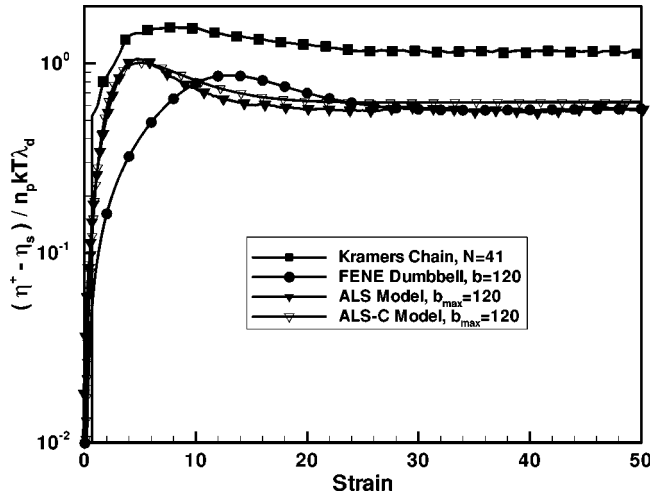


FIG. 17. Dependence of the polymer contribution to the shear stress growth coefficient on shear strain $\gamma \equiv \dot{\gamma}t$ for a 40-rod Kramers chain and the equivalent forms of the FENE dumbbell, FENE-P dumbbell, ALS, and ALS-C models in startup of steady shear flow at $Wi = 11.4$.

predictions for the stress at large strains, as pointed out in Sec. VI, although steady state is reached slightly more slowly for the ALS model. However, at low strains (up to $\epsilon = 2.5$), the FENE dumbbell greatly underpredicts the stress growth in comparison with the Kramers chain. The ALS model corrects this low strain deficiency and is in good agreement with the Kramers chain over the entire range of strains. As argued in Sec. III, the use of the adaptive length scale captures the short length scale dynamics of the Kramers chain that cannot be modeled by the FENE dumbbell.

D. Start-up of steady shear flow

The ability of the ALS model to predict transient rheological properties of a flow containing vorticity is assessed by examining the startup of steady shear flow. Figure 17 shows the evolution of the polymer contribution to the transient shear stress growth coefficient of a 40-link Kramers chain, the equivalent FENE dumbbell, and the equivalent ALS model in startup of steady shear flow at Wi of 11.4. The viscosity of the Kramers chain is twice that of the FENE dumbbell; but even accounting for this difference, the rate of growth of the polymer contribution to the transient viscosity at low strains is much greater for the Kramers chain than for the FENE dumbbell. The ALS model shows a rate of stress growth at low strains that is much greater than that for the FENE dumbbell and much closer to that of the Kramers chain. The overshoot in the polymer contribution to the viscosity of the ALS model also occurs in the same range of strain ($2 < \gamma \equiv \dot{\gamma}t < 20$) as for the Kramers chain. In contrast, the overshoot in the polymer contribution to the viscosity of the FENE dumbbell occurs at much larger strains ($10 < \gamma < 28$). The similarity of the transient behavior between the new model and Kramers chain at low strains shows that the ALS model captures effects due to submolecular length scales in flows with vorticity. This is because the flow strength $\dot{\epsilon}_g$ is equal to 5.7 for a shear flow at $Wi = 11.4$ according to Eq. (31). Substituting this value of $\dot{\epsilon}_g$ into Eq. (29) yields a value of $b_{\text{seg}}^* < b_{\text{max}}$. Therefore, the ALS model behaves as though it possesses shorter length scale modes than the equivalent FENE dumbbell, and this leads to a more rapid growth of shear stress at low strains.

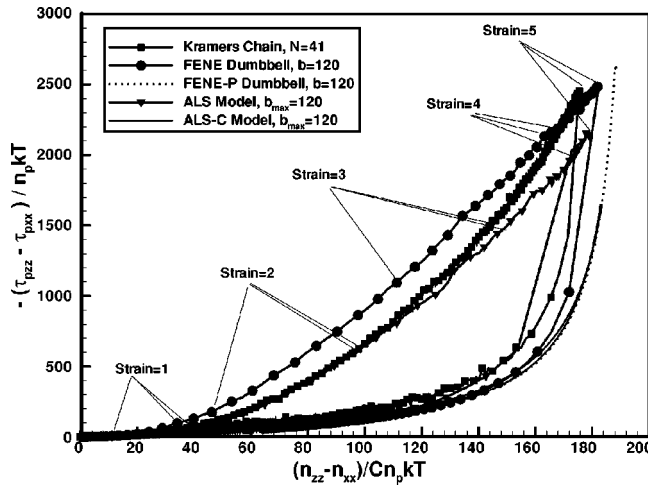


FIG. 18. Stress-birefringence hysteresis plots for a 40-rod Kramers chain and the equivalent forms of the FENE dumbbell, FENE-P dumbbell, ALS, and ALS-C models for startup of a uniaxial extensional flow at $Wi = 11.4$ up to $\epsilon = 5$ and subsequent relaxation.

E. Stress-conformation hysteresis

Stress-birefringence hysteresis is plotted in Fig. 18 for a 40-link Kramers chain, the equivalent FENE dumbbell, and the equivalent ALS model. A uniaxial extensional flow with $Wi = 11.4$ was applied up to $\epsilon = 5$ before the flow was stopped and the polymer solution allowed to relax. The overall shape of the hysteresis loop is similar for all three models, although the size of the loop is slightly smaller for the ALS model than for the FENE dumbbell or the Kramers chain. This is because the ALS model slightly underpredicts the rate of stress growth at intermediate strains ($3 \leq \epsilon \leq 5$) compared to the other two models. Additionally, for a given birefringence, the ALS model predicts a larger stress than the other two models.

As pointed out in Ghosh *et al.* (2001), an important factor for comparison with experiments is the speed with which the loop is traversed. It can be seen in Fig. 18 that the ALS model traverses its hysteresis loop at a rate very similar to the Kramers chain up to $\epsilon = 4$. In the same range of strains, the FENE dumbbell traverses its hysteresis loop at a much slower rate.

F. Planar elongational flow

Planar elongation flow ($\nu_x = -\dot{\epsilon}x, \nu_y = 0, \nu_z = +\dot{\epsilon}z$) deserves consideration, because it arises in many important, complex geometries such as near the forward and rear stagnation points of flow around a cylinder and in extrusion of films. Stress growth for a 40-link Kramers chain and equivalent FENE dumbbell and ALS models were compared for inception of steady planar elongational flow at $Wi = 11.4$. As in uniaxial elongational flow, the FENE dumbbell model predicts a much lower rate of stress growth than the Kramers chain, whereas the ALS model gives much better agreement with the Kramers chain.

VIII. AN APPROXIMATE FORM OF THE ALS MODEL

A closed form approximation of the ALS model is next developed in order to make use of the improved description of extensional rheology feasible in the numerical simulation

of complex flows. A closed form version of the ALS model that is consistent with kinetic theory would ideally be developed as follows. First, the Fokker–Planck equation that is equivalent to the governing equations of the ALS model [Eqs. (29), (36), and (37)] would be derived by using the Fokker–Planck/stochastic differential equation equivalence theorem outlined in Ottiger (1996). The equivalence theorem states that a stochastic differential equation of the form

$$d\mathbf{X}_t = \mathbf{A}(t, \mathbf{X}_t) dt + \mathbf{B}(t, \mathbf{X}_t) \cdot d\mathbf{W}_t \quad (48)$$

is equivalent to the Fokker–Planck equation

$$\frac{\partial}{\partial t} \psi(\mathbf{x}, t) = - \frac{\partial}{\partial \mathbf{x}} \cdot [\mathbf{A}(\mathbf{x}, t) \psi(\mathbf{x}, t)] + \frac{1}{2} \frac{\partial}{\partial \mathbf{x}} \frac{\partial}{\partial \mathbf{x}} : [\mathbf{D}(\mathbf{x}, t) \psi(\mathbf{x}, t)], \quad (49)$$

where

$$\mathbf{D}(\mathbf{x}, t) = \mathbf{B}(\mathbf{x}, t) \cdot \mathbf{B}^T(\mathbf{x}, t). \quad (50)$$

For the ALS model, the set of dependent variables denoted by \mathbf{X}_t consists of the three components of the end-to-end vector and the scalar variable b_{seg} . Next, an evolution equation for the configuration tensor would be obtained by multiplying the Fokker–Planck equation by $\mathbf{Q}\mathbf{Q}$ and integrating over the configuration space.

It is difficult to find the Fokker–Planck form of the ALS model by using this procedure, because $\mathbf{B}(\mathbf{x}, t)$ for the ALS model will contain the coefficient of the Wiener process in Eq. (37), $\sqrt{Kb_{\text{seg}}/b_{\max}}$, which is a complicated function of the variable b_{seg} . Second derivatives of this drag coefficient are taken in the second term on the right side of the Fokker–Planck equation, Eq. (49), and yield a series of yet more complicated terms. An evolution equation for the configuration tensor that is derived from this Fokker–Planck equation would be cumbersome as a result of these terms.

In this paper, we avoid the above procedure by proposing closed form versions of each of the governing equations, such that the properties of the approximate and original forms of the ALS model are similar. First, in the equation for the adaptive length scale [Eq. (29)], the square of the end-to-end distance of an individual molecule is replaced by the trace of the configuration tensor, $\langle \mathbf{Q}\mathbf{Q} \rangle$, and b_{seg}^* is replaced by $\langle b_{\text{seg}}^* \rangle$ to give

$$\frac{\text{Wi}}{K^*} \left(1 - \frac{\text{tr} \langle \hat{\mathbf{Q}}\hat{\mathbf{Q}} \rangle}{\langle b_{\text{seg}}^* \rangle} \left(\frac{b_{\max}}{\langle b_{\text{seg}}^* \rangle} \right) \right) = Z. \quad (51)$$

This approximation is in the same spirit as the Peterlin approximation for the FENE dumbbell, because the distribution function of the end-to-end vector \mathbf{Q} and the distribution of b_{seg}^* are approximated by delta functions. Consequently, the behavior of each individual molecule is not important. Instead, the behavior of the configuration tensor and the average quantity $\langle b_{\text{seg}}^* \rangle$ is computed. A similar Peterlin-type approximation may be applied to the evolution equation for the adaptive length scale [Eq. (36)]. In this case, the distribution function for b_{seg} is assumed to be a delta function, and instead of considering the evolution of b_{seg} for individual molecules, the evolution of the ensemble-averaged quantity $\langle b_{\text{seg}} \rangle$ is computed. In addition, the components of the end-to-end vector \mathbf{Q} are approximated by the square root of the diagonal elements of the configuration tensor $\langle \mathbf{Q}\mathbf{Q} \rangle$ in a Cartesian coordinate system. After incorporating these simplifications, the evolution equation for the adaptive length scale in dimensionless form is

$$\frac{d\langle b_{\text{seg}} \rangle}{d\hat{t}} = - \left| \mathbf{n} \times \begin{pmatrix} \langle \hat{Q}_1 \hat{Q}_1 \rangle^{1/2} \\ \langle \hat{Q}_2 \hat{Q}_2 \rangle^{1/2} \\ \langle \hat{Q}_3 \hat{Q}_3 \rangle^{1/2} \end{pmatrix} \frac{1}{(\text{tr}(\hat{\mathbf{Q}}\hat{\mathbf{Q}}))^{1/2}} \right| \text{Wi}^{\text{eff}} \left(1 - \frac{\text{tr}(\hat{\mathbf{Q}}\hat{\mathbf{Q}})}{\langle b_{\text{seg}}^* \rangle} \frac{b_{\text{max}}}{\langle b_{\text{seg}}^* \rangle} \right) \\ \times (\langle b_{\text{seg}} \rangle - \langle b_{\text{seg}}^* \rangle) K^* + (b_{\text{max}} - \langle b_{\text{seg}} \rangle) K. \quad (52)$$

An alternative approximation of the end-to-end vector \mathbf{Q} is the eigenvector of the configuration tensor $\langle \mathbf{Q}\mathbf{Q} \rangle$ that corresponds to the largest eigenvalue. We do not choose this approach, because a vector composed of the diagonal elements of $\langle \mathbf{Q}\mathbf{Q} \rangle$ in a Protean coordinate system provides a better interpretation of the average orientation of the molecules in several situations. For example, once the system is perturbed from equilibrium in startup of steady uniaxial elongational flow, the principal eigenvector of $\langle \mathbf{Q}\mathbf{Q} \rangle$ is always directed along the principal stretching direction, regardless of the degree of orientation of the molecules with the stretching direction. However, a vector composed of the diagonal elements of $\langle \mathbf{Q}\mathbf{Q} \rangle$ expressed in a Protean coordinate system, is initially oriented at 45° to each of the coordinate axes, but *systematically* rotates towards the principal stretching direction as the molecules become oriented in that direction. This better describes the actual response of the molecules during startup of steady elongational flow.

Finally, an evolution equation for the configuration tensor is derived from the stochastic differential equation for the motion of a segment [Eq. (37)] by simplifying the two-stage procedure outlined above. The first simplification is made during the transformation of the stochastic differential equation into a Fokker-Planck equation. In this step, the length of the segment L is assumed constant, and therefore, the drag coefficient ζ_{seg} and the spring constant H_{seg} are also constant. Following this approximation, the Fokker-Planck equation for a segment of the ALS model is identical to that for the FENE dumbbell except that in the term for the spring force, the maximum extension of the molecule, Q_{od} , is replaced by L . This Fokker-Planck equation is then multiplied by $\mathbf{Q}\mathbf{Q}$ and integrated over the configuration space. Finally, the Peterlin approximation is applied to obtain an expression for the evolution of $\langle \mathbf{Q}\mathbf{Q} \rangle$ in dimensionless form

$$\frac{d\langle \hat{\mathbf{Q}}\hat{\mathbf{Q}} \rangle}{d\hat{t}} = \text{Wi} \{ \hat{\boldsymbol{\kappa}} \cdot \langle \hat{\mathbf{Q}}\hat{\mathbf{Q}} \rangle + \langle \hat{\mathbf{Q}}\hat{\mathbf{Q}} \rangle \cdot \hat{\boldsymbol{\kappa}}^\dagger \} - \frac{K \langle \hat{\mathbf{Q}}\hat{\mathbf{Q}} \rangle}{\left(1 - \frac{\text{tr}(\hat{\mathbf{Q}}\hat{\mathbf{Q}})}{\langle b_{\text{seg}} \rangle} \left(\frac{b_{\text{max}}}{\langle b_{\text{seg}} \rangle} \right) \right)} + K \left(\frac{\langle b_{\text{seg}} \rangle}{b_{\text{max}}} \right) \boldsymbol{\delta}. \quad (53)$$

Although the length of the segment is assumed constant in transforming the stochastic differential equation for the motion of the segment, L is taken to be a variable. Hence, the governing equations of the closed form of the ALS model, which consist of Eqs. (51), (52), and (53), allow the adaptive length scale to evolve according to the kinematic history in a similar fashion to the unapproximated version of the ALS model. We refer to the closed form of the ALS model as the ALS-C model.

Expressions for the stress and the birefringence of the ALS-C model are obtained by applying the same approximations that are used to simplify the governing equations for the microstructure as outlined above. Therefore, Eq. (38) for the stress is simplified to

$$\hat{\tau}_p = \frac{b_{\max}}{\langle b_{\text{seg}} \rangle} \boldsymbol{\delta} + \left(\frac{b_{\max}}{\langle b_{\text{seg}} \rangle} \right)^2 \frac{\langle \hat{\mathbf{Q}} \hat{\mathbf{Q}} \rangle}{\left(1 - \frac{\text{tr} \langle \hat{\mathbf{Q}} \hat{\mathbf{Q}} \rangle}{\langle b_{\text{seg}} \rangle} \left(\frac{b_{\max}}{\langle b_{\text{seg}} \rangle} \right) \right)} \quad (54)$$

and Eq. (39) for birefringence becomes

$$\Delta n = \frac{5}{3} C n_p k T \left(\frac{b_{\max}}{\langle b_{\text{seg}} \rangle} \right)^2 \langle (\hat{Q}_z \hat{Q}_z - \hat{Q}_x \hat{Q}_x) \rangle. \quad (55)$$

In the remainder of this section, the properties of the ALS-C model are compared with the results of the unapproximated version. First, the uniaxial elongational viscosity of the closed and unapproximated versions of the ALS model is presented in Fig. 11. For large Wi, the elongational viscosity of the ALS-C model agrees with the 100-link Kramers chain, equivalent FENE dumbbell, and equivalent ALS model. Below the coil-stretch transition, the ALS-C model is also in good agreement with the ALS and FENE dumbbell models.

The viscometric properties of the ALS-C model are compared in Figs. 12 and 13 with a 100-link Kramers chain and the equivalent FENE dumbbell and ALS models. These figures demonstrate that the ALS-C model predictions for these properties tend to those of the FENE-P model for $\text{Wi} \gg 1$. To understand how closure leads to this behavior, the dependencies of $\langle b_{\text{seg}} \rangle$ on Wi for the ALS-C and ALS versions of the model are compared in Fig. 14. Whereas $\langle b_{\text{seg}} \rangle$ for the ALS model decreases rapidly for $2 < \text{Wi} < 100$ before leveling off to a value of $\langle b_{\text{seg}} \rangle = 150$ at large Wi, for the ALS-C model $\langle b_{\text{seg}} \rangle$ decreases rapidly to a minimum for $2 < \text{Wi} < 10$ before increasing back to b_{\max} at large Wi. As a result, the values of the polymer contribution to the viscosity and the first normal stress coefficient for the ALS-C model approach the predictions of the FENE-P dumbbell model in the shear-thinning regime.

The predictions for the startup of steady uniaxial elongational flow of the ALS-C model are compared in Fig. 16 with those of a 40-link Kramers chain, the equivalent FENE dumbbell, and the equivalent ALS model. The ALS-C model behaves similarly to the ALS model; the only difference is that the ALS-C model displays a knee as the stress approaches steady state. The knee is characteristic of the Peterlin closure approximation [van den Brule (1993)]; and it is prominent for the FENE-P dumbbell, which also is shown in Fig. 16.

Figure 17 compares stress growth in the startup of steady shear flow for a 40-link Kramers chain with the equivalent FENE dumbbell, ALS, and ALS-C models at a Weissenberg number of 11.4. The polymer contribution to the shear stress growth coefficient η_p^+ of the ALS-C model is very similar to those of the Kramers chain and the ALS model up to a shear strain of 2. This demonstrates that closure does not affect the ability of the ALS model to describe short length scale behavior in a flow with vorticity. As observed for the Kramers chain and the ALS model, the ALS-C model exhibits overshoot between shear strains of 2 and 20. However, the ALS-C model reaches a steady-state value slightly greater than those of the FENE dumbbell and ALS models. The relation of the viscometric properties of 40-link Kramers chains to the equivalent FENE dumbbell and ALS models is similar to the relation of the viscometric properties of 100-link Kramers chains to the equivalent FENE dumbbell and ALS models. Thus the viscosity for the ALS-C model at $\text{Wi} = 11.4$ in Fig. 17 is consistent with the results presented in Fig. 12.

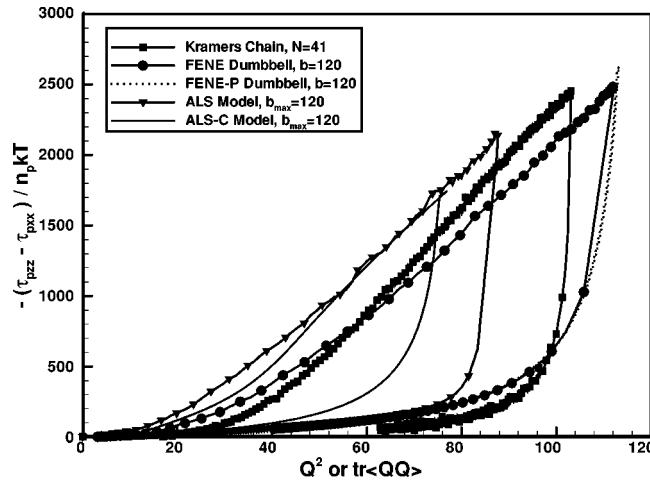


FIG. 19. Stress-confirmation hysteresis plots for a 40-rod Kramers chain and the equivalent forms of the FENE dumbbell, ALS, and ALS-C models for inception of steady uniaxial extensional flow at $Wi = 11.4$ up to $\epsilon = 5$ and subsequent relaxation. Stress is plotted against mean square extension.

The predictions for stress-conformation hysteresis are shown in Fig. 18 for the ALS-C model. For a FENE dumbbell, hysteresis arises solely because of hysteresis in the distribution function. The distribution function assumes very different shapes during extension and relaxation, which leads to multiple values of stress for a given birefringence [Lielens *et al.* (1999)]. When the Peterlin approximation is used with the FENE dumbbell equations, the distribution function is approximated as a delta function, leading to a one-to-one relationship between stress and birefringence and the elimination of hysteresis [Sizaire *et al.* (1999)]. However, the ALS model exhibits configurational hysteresis as well as hysteresis in the distribution function. The latter hysteresis arises for the same reasons as in the FENE dumbbell. Configurational hysteresis arises because polymer molecules with given end-to-end distances assume different internal configurations during extension and relaxation. The FENE dumbbell cannot capture configurational hysteresis, because its internal configuration is completely described by the end-to-end vector. In contrast, for a given end-to-end distance as shown in Fig. 19, the ALS model can predict a range of possible adaptive length scales, specified by b_{seg} , which is a crude representation of internal configuration. Configurational hysteresis arises in the ALS model, because the evolution of $\langle b_{\text{seg}} \rangle$ is different during extension and relaxation. Applying a closure approximation to obtain the ALS-C model approximates the distribution function for the end-to-end distance with a delta function and removes the hysteresis in the distribution function. However, applying a closure approximation to the new model in this way very nearly removes stress-birefringence hysteresis as shown in Fig. 18. Apparently configurational hysteresis in the closed form of the model is not sufficient to produce significant stress-birefringence. This may be due to the fact that the total birefringence of the molecule is a sum of segmental contribution as seen in Eqs. (39) and (55); two different configurations (such as highly kinked or fully unraveled) could lead to similar birefringence. If the mean square extension, which could be more sensitive to configuration of the molecules, is used, however, the closed version of the new model displays hysteresis. This hysteretic behavior is strictly due to the different configurations during stretching or relaxation, because the distributional hysteresis is removed due to the closure approximation.

Finally, the behavior of the ALS-C model in planar elongational flow at $Wi = 11.4$ is compared with that of a 40-link Kramers chain and the equivalent FENE dumbbell and ALS models. We find that the ALS-C model is in close agreement with the Kramers chain and ALS model. All three models predict much faster stress growth up to $\epsilon = 2.5$ than given by the FENE dumbbell model.

IX. CONCLUSIONS

A new model for dilute polymer solutions has been developed that captures much of the physics of the Kramers chain in a wide range of flows through the addition of only one additional configurational variable, an *adaptive length scale* b_{seg} . This model is tractable because of several important simplifications inspired by insights into important aspects of polymer dynamics found by studying the behavior of Kramers chains. In particular, the definition of an adaptive length scale allows the model to capture behavior across a range of length scales, while using only one configuration variable \mathbf{Q} to describe molecular extension and orientation.

The ALS model successfully replicates the behavior of Kramers chains in steady and transient extensional flows. It also describes the stress-birefringence hysteresis of the Kramers chain in the startup of and relaxation following steady uniaxial elongational flow. Other coarse-grained models such as the FENE dumbbell [Doyle *et al.* (1998a, 1998b); Ghosh *et al.* (2001)] or the Verhoef model [Verhoef *et al.* (1999)] do not describe simultaneously both sets of features. Although not done within a rigorous kinetic theory framework, a closed form of the ALS model—the ALS-C model—is also developed that is convenient for complex flow calculations; the steady and transient extensional properties of the ALS model are nearly unchanged by the closure approximation. Moreover, in contrast to the FENE-P dumbbell model, stress-conformation hysteresis is preserved in the ALS-C model. This is because the ALS model can account for configurational hysteresis through the variable b_{seg} as well as capture hysteresis in the distribution function [Keunings (1997)] of the kind present in the FENE dumbbell. Since the Peterlin closure eliminates hysteresis in the distribution function, the FENE-P dumbbell shows no hysteresis. However, the ALS-C model exhibits hysteresis due to the configurational hysteresis remaining after the closure approximation is applied.

In steady shear flow, the ALS and ALS-C models shear thin in a fashion similar to the Kramers chain and the FENE or FENE-P dumbbell models. In the startup of steady shear flow, both the original and closed forms of the ALS model show rapid growth in the shear stress at low shear strains that are similar to the corresponding result for the Kramers chain. Hence the new model gives superior descriptions of rheological properties to the FENE and FENE-P dumbbells in a broader class of flows than simply uniaxial and planar extensional flow. The success in predicting transient shear flow properties demonstrates that the ALS model captures short length scale behavior in flows with vorticity.

The ALS model may be a significant improvement for simulating complex flows. In its closed form, the model provides a better physical description of the polymer than a FENE-P dumbbell, with little extra computational effort. Without closure, it is superior to the FENE dumbbell for use in hybrid Brownian dynamics/continuum calculations. In addition, some of the concepts introduced here, such as the adaptive length scale, may be useful in attempts to develop rigorous mapping techniques between fine-grained and coarse-grained models.

ACKNOWLEDGMENT

This work was supported primarily by the ERC Program of the National Science Foundation under Award Number EEC-9731680.

References

- Adachi, K., "Calculation of strain histories in Protean coordinate systems," *Rheol. Acta* **22**, 326–335 (1983).
- Bird R. B., C. F. Curtiss, R. C. Armstrong, and O. Hassager, *Dynamics of Polymeric Liquids. Volume 2: Kinetic Theory*, 2nd ed. (Wiley Interscience, New York, 1987).
- Coates, P. J., R. C. Armstrong, and R. A. Brown, "Calculation of Steady-State Viscoelastic Flow Through Axisymmetric Contraction with the EEME Formulation," *J. Non-Newtonian Fluid Mech.* **42**, 141–188 (1992).
- Doyle, P. S., E. S. G. Shaqfeh, and A. P. Gast, "Dynamic simulation of freely draining flexible polymers in steady linear flows," *J. Fluid Mech.* **334**, 251–291 (1997).
- Doyle, P. S. and E. S. G. Shaqfeh, "Dynamic simulation of freely draining, flexible bead-rod chains: Startup of extensional and shear flow," *J. Non-Newtonian Fluid Mech.* **76**(1), 43–78 (1998a).
- Doyle, P. S., E. S. G. Shaqfeh, G. H. McKinley, and S. H. Spiegelberg, "Relaxation of dilute polymer solutions following extensional flows," *J. Non-Newtonian Fluid Mech.* **76**(1), 79–110 (1998b).
- Flory P. J., *Principles of Polymer Chemistry* (Cornell University Press, New York, 1953).
- Gardiner C. W., *Handbook of Stochastic Methods* (Springer, New York, 1985).
- Ghosh, I., G. H. McKinley, R. A. Brown, and R. C. Armstrong, "Deficiencies of FENE Dumbbell Models in Describing the Rapid Stretching of Dilute Polymer Solutions," *J. Rheol.* **45**, 721–758 (2001).
- Hassager, O., "Kinetic theory and rheology of bead-rod models for macromolecular solutions. I. Equilibrium and steady flow properties," *J. Chem. Phys.* **60**, 2111–2124 (1974).
- Herrchen, M. and H. C. Öttinger, "A detailed comparison of various FENE dumbbell models," *J. Non-Newtonian Fluid Mech.* **68**, 17–42 (1997).
- James, D. F. and T. Sridhar, "Molecular conformation during steady-state measurements of extensional viscosity," *J. Rheol.* **39**, 713–724 (1995).
- Keunings, R., "On the Peterlin Approximation for finitely extensible dumbbells," *J. Non-Newtonian Fluid Mech.* **68**, 85–100 (1997).
- Larson, R. G., H. Hu, D. E. Smith, and S. Chu, "Brownian dynamics simulations of a DNA molecule in an extensional flow field," *J. Rheol.* **43**, 267–304 (1999).
- Lielens, G., R. Keunings, and V. Legat, "The FENE-L and the FENE-LS closure approximations to the kinetic theory of finitely extensible dumbbells," *J. Non-Newtonian Fluid Mech.* **87**, 179–196 (1999).
- Liu, A. W., D. E. Bornside, R. C. Armstrong, and R. A. Brown, "Viscoelastic flow of polymer solutions around a periodic, linear array of cylinders: Comparisons of predictions for microstructure and flow fields," *J. Non-Newtonian Fluid Mech.* **77**, 153–190 (1998).
- Liu, T. W., "Flexible polymer chain dynamics and rheological properties in steady flows," *J. Chem. Phys.* **90**, 5826–5842 (1989).
- Olbright, W. L., J. M. Rallison, and L. G. Leal, "Strong flow criteria based on microstructure deformation," *J. Non-Newtonian Fluid Mech.* **10**, 291–318 (1982).
- Ortiz, C. and G. Hadzianou, "Entropic Elasticity of Single Polymer Chains of Poly(methylacrylic acid) Measured by Atomic Force Microscopy," *Macromolecules* **32**, 78–787 (1999).
- Öttinger H. C., *Stochastic Processes in Polymeric Fluids* (Springer, Berlin, 1996).
- Purnode, B. and M. J. Crochet, "Flows of polymer solutions through contractions part 1: Flows of polyacrylamide solutions through planar contractions," *J. Non-Newtonian Fluid Mech.* **65**, 269–289 (1996).
- Rallison, J. M., "Dissipative stresses in dilute polymer solutions," *J. Non-Newtonian Fluid Mech.* **68**, 61–83 (1996).
- Sizaire, R., G. Lielens, I. Jaumain, R. Keunings, and V. Legat, "On the hysteretic behavior of dilute polymer solutions in relaxation following extensional flow," *J. Non-Newtonian Fluid Mech.* **82**, 233–253 (1999).
- Smith, D. E., H. P. Babcock, and S. Chu, "Single-polymer dynamics in steady shear flow," *Science* **283**, 1724–1727 (1999).
- Talwar, K. K. and B. Khomami, "Flow of viscoelastic fluids past periodic square arrays of cylinders: Inertial and shear thinning viscosity and elasticity effects," *J. Non-Newtonian Fluid Mech.* **57**, 177–202 (1995).
- Tanner, R. I., "A test particle approach to flow classification for viscoelastic fluids," *AICHE J.* **22**, 910–918 (1976).
- Tirtaatmadja, V. and T. Sridhar, "Comparison of constitutive equations of polymer solutions in uniaxial extension," *J. Rheol.* **39**, 1133–1159 (1995).

- van den Brule, B. H. A. A., "Brownian dynamics simulation of finitely extensible bead-spring chains," *J. Non-Newtonian Fluid Mech.* **47**, 357–378 (1993).
- Verhoeven, M. R. J., B. H. A. A. van den Brule, and M. A. Hulsen, "On the modeling of PIB/PB Boger Fluid in extensional flow," *J. Non-Newtonian Fluid Mech.* **80**, 155–182 (1999).
- Wiest, J. M., "Birefringence in strong flows of dilute polymer solutions," *Polymer* **40**, 1917–1922 (1999).